National Center for Sustainable Transportation
A USDOT University Transportation Center

Research Report

April 2025

Understanding Real-World Brake Activity

A Key to Assessing Non-Tailpipe Emission Sources

Guoyuan Wu, University of California, Riverside

Xuanpeng Zhao, University of California, Riverside

Heejung Jung, University of California, Riverside

UCR College of Engineering – Center for Environmental Research and Technology

TECHNICAL REPORT DOCUMENTATION PAGE

1. Report No. NCST-UCR-RR-25-12	**2. Government Accession No.** N/A	**3. Recipient's Catalog No.** N/A
4. Title and Subtitle Understanding Real-World Brake Activity: A Key to Assessing Non-Tailpipe Emission Sources		**5. Report Date** April 2025 **6. Performing Organization Code** N/A
7. Author(s) Guoyuan Wu, Ph.D., https://orcid.org/0000-0001-6707-6366 Xuanpeng Zhao, https://orcid.org/0000-0001-7073-6927 Heejung Jung, Ph.D., https://orcid.org/0000-0001-5864-7358		**8. Performing Organization Report No.** N/A
9. Performing Organization Name and Address University of California, Riverside Bourns College of Engineering – Center for Environmental Research & Technology 1084 Columbia Avenue Riverside, CA 92507		**10. Work Unit No.** N/A **11. Contract or Grant No.** USDOT Grant 69A3552348319 and 69A3552344814
12. Sponsoring Agency Name and Address U.S. Department of Transportation Office of the Assistant Secretary for Research and Technology 1200 New Jersey Avenue, SE, Washington, DC 20590		**13. Type of Report and Period Covered** Final Research Report (March 2024 – February 2025) **14. Sponsoring Agency Code** USDOT OST-R
15. Supplementary Notes DOI: https://doi.org/10.7922/G2HD7T14 Dataset DOI: https://doi.org/10.5061/dryad.41ns1rnrp		

16. Abstract

Understanding and mitigating non-tailpipe emissions, particularly those from braking activities, is crucial for improving air quality and public health. This study investigates the impact of vehicle brake activity on mobile-source particulate matter (PM) emissions at signalized intersections using a multi-modal data collection approach. The research integrates LiDAR-based trajectory detection, roadside camera monitoring, drone surveillance, and in-vehicle sensor data to analyze braking behaviors and their associated emissions. A hybrid physical-machine learning model was developed to detect braking events and estimate brake-induced PM emissions. The methodology involves LiDAR-based vehicle tracking, trajectory refinement, brake activity detection, and brake emission estimation. By leveraging deep learning algorithms for multi-object tracking and data fusion techniques, the study provides a robust framework for real-time brake activity monitoring. The study further incorporates an empirical emissions model, which is calibrated using laboratory dynamometer tests, to estimate brake wear particle emissions based on kinetic energy dissipation. The results demonstrate that braking intensity and frequency significantly influence PM emissions, with variations observed across different brake pad materials. Real-world validation using a probe vehicle dataset confirms the accuracy of the model, achieving high precision (97%) and recall (100%) in braking event detection. The brake emissions estimation model effectively quantifies PM10 emissions, with calibrated emission factors highlighting material-specific variations. Findings from this research underscore the importance of accounting for non-tailpipe emissions in urban air quality management and regulatory policies. The proposed methodology provides a scalable, non-intrusive solution for monitoring braking-induced emissions in real-world traffic conditions. Future research should explore the integration of regenerative braking impacts, powertrain differentiation, and further refinements in sensor fusion techniques to enhance emission inventory accuracy and inform transportation policy development.

17. Key Words Brake activity prediction, brake wear emissions, advanced roadside sensing, sensor fusion		**18. Distribution Statement** No restrictions.	
19. Security Classif. (of this report) Unclassified	**20. Security Classif. (of this page)** Unclassified	**21. No. of Pages** 55	**22. Price** N/A

Form DOT F 1700.7 (8-72) Reproduction of completed page authorized

About the National Center for Sustainable Transportation

The National Center for Sustainable Transportation is a consortium of leading universities committed to advancing an environmentally sustainable transportation system through cutting-edge research, direct policy engagement, and education of our future leaders. Consortium members include: the University of California, Davis; California State University, Long Beach; Georgia Institute of Technology; Texas Southern University; the University of California, Riverside; the University of Southern California; and the University of Vermont. More information can be found at: ncst.ucdavis.edu.

Disclaimer

The contents of this report reflect the views of the authors, who are responsible for the facts and the accuracy of the information presented herein. This document is disseminated in the interest of information exchange. The report is funded, partially or entirely, by a grant from the U.S. Department of Transportation's University Transportation Centers Program. However, the U.S. Government assumes no liability for the contents or use thereof.

The U.S. Department of Transportation requires that all University Transportation Center reports be published publicly. To fulfill this requirement, the National Center for Sustainable Transportation publishes reports on the University of California open access publication repository, eScholarship. The authors may copyright any books, publications, or other copyrightable materials developed in the course of, or under, or as a result of the funding grant; however, the U.S. Department of Transportation reserves a royalty-free, nonexclusive and irrevocable license to reproduce, publish, or otherwise use and to authorize others to use the work for government purposes.

Acknowledgments

This study was funded, partially or entirely, by a grant from the National Center for Sustainable Transportation (NCST), supported by the U.S. Department of Transportation (USDOT) through the University Transportation Centers program. The authors would like to thank the NCST and the USDOT for their support of university-based research in transportation, and especially for the funding provided in support of this project. The authors would like to thank Chuheng Wei and Ziyan Zhang for their support in data collection, and Ajay Anubolu for his contribution in data labeling.

Understanding Real-World Brake Activity: A Key to Assessing Non-Tailpipe Emission Sources

A National Center for Sustainable Transportation Research Report

Guoyuan Wu, Center for Environment Research & Technology, Department of Electrical & Computer Engineering, University of California, Riverside

Xuanpeng Zhao, Department of Electrical & Computer Engineering, University of California, Riverside

Heejung Jung, Center for Environment Research & Technology, Department of Mechanical Engineering, University of California, Riverside

Table of Contents

List of Figures

Understanding Real-World Brake Activity: A Key to Assessing Non-Tailpipe Emission Sources

Executive Summary

Introduction

Transportation-related emissions have long been a major environmental and public health concern, with a significant focus on tailpipe pollutants. However, non-tailpipe emissions—especially those from brake and tire wear—are becoming a larger fraction of mobile-source particulate matter (PM) emissions. Among these, brake wear emissions at intersections are a growing concern due to frequent stopping and braking activities, leading to localized air pollution hotspots. This study investigates the impact of brake activity on mobile-source PM emissions at signalized intersections, leveraging advanced sensing technologies and hybrid physical-machine learning models to enhance real-world brake emission monitoring.

Methodology

This research utilizes multi-modal data collection techniques, integrating:

1. Light Detection and Ranging (LiDAR) based vehicle detection, localization and classification to extract high-resolution trajectory;
2. Roadside and drone-based video monitoring to determine the braking events;
3. In-vehicle sensors (i.e., Global Positioning System (GPS), on-board diagnostic or OBD-II system) for brake pressure measurements to provide ground truth of brake activity; and
4. Machine learning and physical modeling for brake activity prediction and PM emissions estimation, considering different brake pad materials.

More specifically, the approach involves:

1. *Trajectory Detection* and *Refinement* by fusing roadside LiDAR and video feeds, thus vehicle movements are tracked with high precision.
2. *Brake Activity Identification* by leveraging a hybrid model (i.e., combining data-driven and model-based methods) to predict braking events and intensity based on refined vehicle trajectories.
3. *Brake Wear Emission Estimation* based on the kinetic energy dissipation during braking for estimating PM emissions, where parameters have been calibrated with laboratory dynamometer test data.

Key Findings

The key findings of the research are summarized below:

1. The hybrid brake activity identification model achieved 97% precision and 100% recall in detecting braking events when validated against real-world probe vehicle data. This shows great potential of the proposed approach for highly accurate brake event and intensity prediction.
2. Brake pad materials significantly affect PM10 emissions, with European Commercial Exchange (ECE) pads generating the highest emissions, while Non-Asbestos Organic (NAO) pads have the lowest.
3. Signalized intersections were found to amplify braking-induced emissions, highlighting the need for targeted emission reduction strategies.
4. Real-world brake wear emissions data can inform transportation policies, supporting initiatives to mitigate non-tailpipe emissions through materials regulation, adaptive traffic signal control, and sustainable urban planning.

Conclusions and Recommendations

This research provides a scalable, non-intrusive method for monitoring and analyzing brake wear emissions in real-world traffic conditions. Findings emphasize the importance of non-tailpipe emissions in air quality management and call for: a) *Regulatory Considerations* for brake material standards to minimize PM emissions; b) *Traffic Signal Optimization* to reduce unnecessary braking at intersections; and c) *Integration with Electric Vehicles* (EVs) and regenerative braking to further mitigate brake wear emissions.

Future research should expand on vehicle powertrain differentiation, explore real-world impacts of regenerative braking, and refine sensor fusion methodologies to enhance the accuracy and applicability of non-tailpipe emission monitoring systems.

Introduction

On-road vehicles (e.g., cars, buses, trucks) emit inhalable particles, which may cause adverse health effects, from two major sources: one is the exhaust system via the tailpipe, while the other is non-exhaust source such as brake wear, tire/road wear, clutch wear and road dust resuspension. The former has been extensively characterized and regulations have been taking effects on reducing those diesel and gasoline exhaust particulate emissions over the past decades (e.g., Truck and Bus). Compared to tailpipe emissions, much less research has been conducted on non-exhaust emissions and no regulations have been applied to them, mainly due to the challenges in measurement and control.

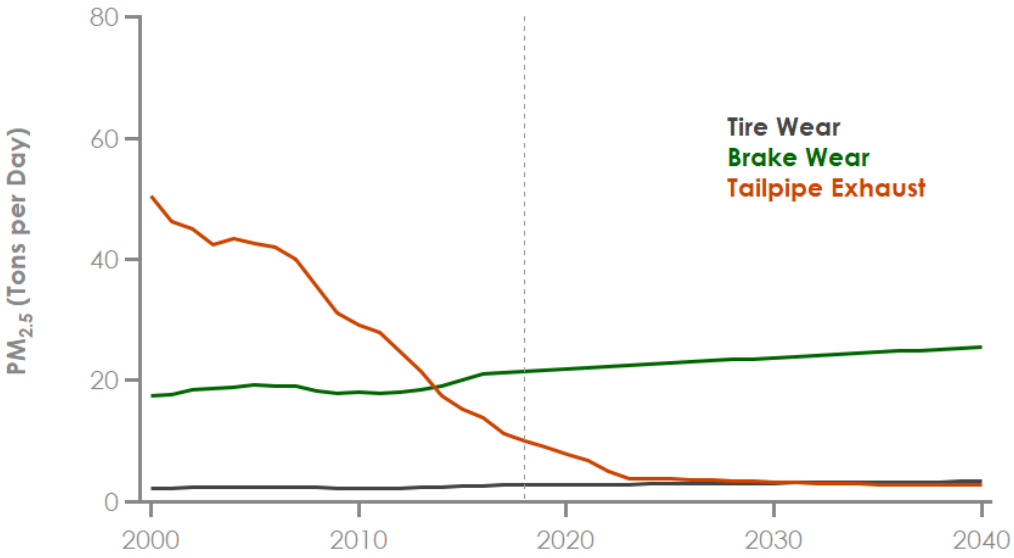

Figure 1. PM2.5 emissions predicted with EMFAC2017 (courtesy of CARB).

A recent study funded from California Air Resource Board (CARB) found out that the contribution of non-tailpipe particulate emissions has already exceeded that of tailpipe particulate emissions in California highways in 2020. This is consistent with CARB's internal calculation using the updated Emission Factors (EMFAC), as shown in Figure 1. The on-going electrification of transportation systems and zero-emission vehicle campaigns are expected to lead to much more disproportionately higher fraction of non-tailpipe particulate emissions compared to the current and past. In addition, brake and tire wear particles are composed of various metals, rubber compounds, and organics which includes adhesives. The severity of their health effect has not been studied in detail yet, but a recent study indicated high correlation between antioxidant depletion and non-tailpipe emissions factors (especially non-tailpipe brake events) based on receptor modeling (see Figure 2).

To further investigate the brake and tire wear related impact, it is of importance to build up a comprehensive emissions inventory which is the major goal of this project. However, most of the existing emission inventory is calculated from the speed-corrected emissions factors determined from the laboratory study using a brake dynamometer, which is a type of inertia dynamometer. This calculation has major uncertainties thus may not be reliable for the basis of regulation or policy enactment, because realistic brake activities/maneuvers have not been properly accounted for. One of the key challenges lie in the absence of real-world brake activity measurements (note that road wear, tire wear, and brake wear emissions occur during braking, while tire and road wear emissions occur during acceleration events).

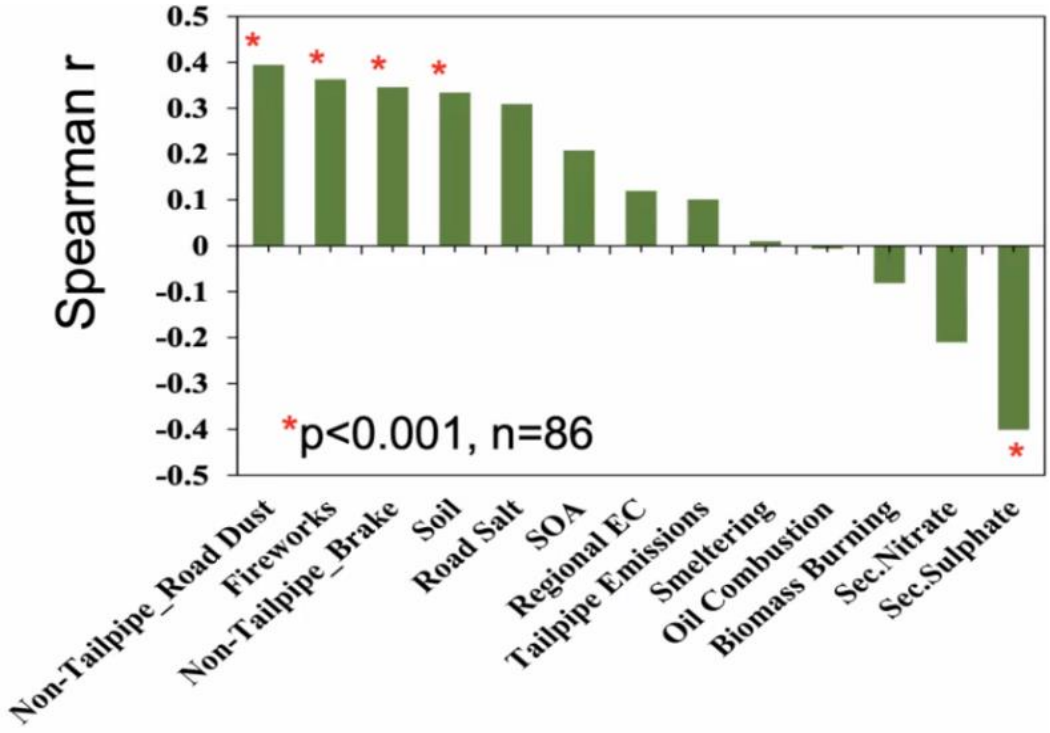

Figure 2. Spearman correlation between antioxidant depletion and different emissions factors (courtesy of Dr. Greg Evans, University of Toronto).

To address the aforementioned real-world brake activity data gaps, the research team in this project has leveraged multiple data sources to collect and measure real-world brake activities of vehicles traversing signalized intersections. These data sources include advanced infrastructure-based sensing technologies, e.g., LIDAR and high definition (HD) camera, drone surveillance and probe vehicle. Deep learning-based computer vision algorithms have been utilized to perform data mining, spatio-temporal synchronization, sensor fusion, vehicle detection and localization, and multi-object tracking. This method is non-intrusive and shows potential to collect massive high-resolution vehicle trajectories in the real world. In addition, by fusing data from different sources (e.g., in-vehicle sensors and roadside sensors), brake activities and even brake intensities can be estimated/predicted, based on the roadside surveillance results. Therefore, this method is

also promising to create a database of real-world brake activities for a large volume of vehicles, which is of importance to build up a comprehensive brake-induced emissions inventory.

The rest of this report is organized as follows. Section 2 reviews the pertinent studies on high-resolution trajectory detection (mainly by LiDAR), brake activity prediction from trajectories, and brake emission estimation. Section 3 details the methodology used to collect and estimate/predict real-world brake activity, including the workflow and respective modules. The data collection efforts and preliminary case study results are presented in Section 4. The last section concludes this project with further discussion.

Literature Review

The literature review examines trajectory detection methods (mainly using LiDAR and focusing on advanced deep learning algorithms for multi-object tracking and cooperative perception frameworks), brake activity detection leveraging trajectory data from diverse sources, and modeling of brake emissions with an emphasis on energy dissipation, material composition, and temperature sensitivity. This comprehensive review synthesizes findings from recent studies to identify gaps in existing research and establish a foundation for developing more precise and integrated approaches to addressing challenges in vehicle trajectory analysis, braking behavior prediction, and non-exhaust particulate matter emissions modeling.

LiDAR-based trajectory detection

Trajectory detection using LiDAR has been extensively studied to address challenges such as occlusion, limited sensing range, and accurate tracking in complex traffic environments. Advanced methods, e.g., ResNet18-based architecture [1], have demonstrated high precision in vehicle detection and multi-object tracking (MOT). By leveraging bird's-eye view (BEV) mapping and an enhanced Hungarian algorithm, this approach achieves F1-scores of 96.97% and MOT of 88.12% on the Karlsruhe Institute of Technology and Toyota Technological Institute (KITTI) dataset, effectively addressing occlusion issues and ensuring robust trajectory reconstruction. Similarly, cooperative perception frameworks such as PillarGrid [2], have shown significant improvements in object detection by fusing multi-source and multi-modal sensor data (e.g., onboard and roadside LiDAR data) using deep learning pipelines, achieving up to 90% improvement in accuracy over single-sensor systems. Additionally, behavior classification frameworks [3] have explored the use of Hidden Markov Models (HMM) combined with Bayesian Filtering to classify turning movements at intersections, which may affect braking activity characteristic in the real world.

In this project, we adopted the Cyber Mobility Mirror (CMM) framework [4] due to its practical design and alignment with our goal of collecting real-world trajectory data for non-tailpipe emissions modeling. The CMM system employs a modular pipeline that integrates Roadside Data Transformation (RDT), lightweight 2D voxelization on the x-y plane, and efficient feature extraction via a Feature Pyramid Network (FPN) architecture (see Figure 3). These design choices enable reliable object detection and tracking without significant computational demands. Field tests validate its performance with detection precision of 96.99% and recall of 83.62%, along with minimal geo-localization errors (0.69m lateral, 0.33m longitudinal) [4]. While advanced methods, e.g., ResNet18-based architectures, offer higher precision under controlled conditions, CMM's adaptability and modular design provide an effective balance between performance and feasibility, ensuring that the project meets its objectives.

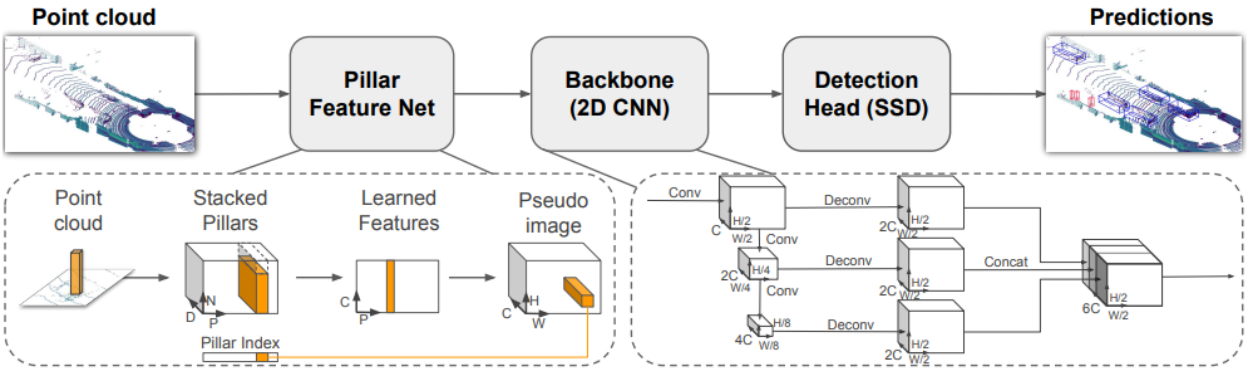

Figure 3. Network architecture of PointPillars adopted in the CMM framework of this project.

Trajectory-based brake activity estimation

The detection of braking activity and the estimation of brake-induced deceleration using trajectory data have been explored through various methodologies, leveraging diverse data sources such as smartphone sensors, GPS, LiDAR, and video-based trajectory analysis. Smartphone-based systems, such as the "Nericell" framework [5], utilize accelerometer and GPS data to detect braking events by reorienting accelerometer readings to align with the vehicle's axes and identifying surges in forward acceleration. This method effectively detects braking activity and estimates deceleration indirectly based on changes in acceleration along the vehicle's forward axis, but does not directly measure precise deceleration values or provide continuous braking intensity metrics. GPS-based algorithms [6] adopt a trajectory-based approach by calculating velocity and acceleration from positional data using the Haversine formula, although the positional accuracy would significantly impact the algorithm performance. These methods detect braking events when deceleration exceeds a predefined threshold and classify them into binary states (braking or not braking). While cost-effective and achieving reasonable accuracy, their reliance on discrete thresholds limits their ability to provide continuous deceleration profiles or quantify braking intensity beyond event detection. Leveraging LiDAR's 3D detection capabilities, LiDAR-based approaches [7] further enhance trajectory-based methods by incorporating advanced deep learning models, such as hybrid Convolutional Neural Network and Gated Recurrent Unit (CNN-GRU) architectures, which analyze vehicle trajectories to predict near-crash events based on deceleration thresholds and kinetic energy reduction. Although highly accurate for event classification, these methods focus on binary outcomes (normal vs. near-crash) and do not estimate brake-induced deceleration or continuous intensity metrics. Video-based trajectory analysis [8] introduces another trajectory-focused method by employing adaptive segmented linear fitting to analyze vehicle motion parameters derived from surveillance footage. This approach calculates velocity and direction variation rates at trajectory inflection points to detect sharp braking, turning, or combined behaviors. While effective for identifying high-risk behaviors, it provides only indirect insights into deceleration through velocity variation

rates and does not measure physical deceleration values directly. It is noted that compared to LiDAR technology, it is more challenging for video camera to provide higher 3D positional accuracy or better depth estimation from 2D images.

Across these studies, a common limitation is the reliance on indirect indicators of brake-induced deceleration rather than direct measurements. None of the reviewed methods explicitly isolate brake-induced deceleration from other forms of deceleration, such as coasting or regenerative braking. This gap highlights an opportunity for future research to explore the use of brake pressure data in training models that can predict brake-induced deceleration with greater precision. Such an approach could enhance current methodologies by offering more detailed insights into braking dynamics while maintaining the advantages of trajectory-based detection systems.

Brake emission estimation by brake activity

The modeling of brake emissions is a complex task that requires a comprehensive understanding of the factors contributing to particulate matter (PM) generation during braking events. Studies have consistently identified brake system characteristics, operational conditions, and energy dissipation as critical contributors to brake wear emissions [9][10][11][12]. By synthesizing insights from laboratory experiments, real-world driving data, and advanced analytical techniques, researchers have developed methodologies to quantify and model these emissions. This section explores the main contributors to brake emissions and how they can be integrated into a robust modeling framework.

A key contributor to brake emissions is the energy dissipated during braking, which directly influences wear rates and particle generation [9][11][13][14]. During braking, the kinetic energy of a moving vehicle is converted into thermal energy through friction between the brake pad and rotor. The magnitude of this energy dissipation depends on factors such as vehicle speed, deceleration rates, and braking force distribution. For example, studies using real-world driving cycles, such as the Worldwide Harmonized Light-Duty Vehicles Test Procedure (WLTP), World-wide harmonized Light duty Test Cycle (WLTC), or Urban Driving Program (UDP), have shown that higher deceleration rates and initial speeds lead to greater energy dissipation, resulting in increased wear (on both brake and tire) and higher PM emissions [11][15]. Aggressive braking scenarios, such as those simulated in the AMS (Aggressive Braking Scenarios) tests, further amplify this effect by generating disc temperatures exceeding 500°C, which enhance both mechanical abrasion and volatilization processes [13][16]. These findings underscore the necessity of incorporating energy dissipation metrics into brake emission models to capture variations in braking intensity across different driving conditions.

Energy dissipation also plays a pivotal role in determining particle size distributions [17][18][19]. Mild braking events typical of urban driving cycles tend to produce finer particles (<2.5 μm), which dominate number-weighted size distributions due to lower

energy dissipation rates. In contrast, high-energy braking events associated with aggressive deceleration generate larger particles (>10 μm) due to increased mechanical fragmentation at elevated temperatures [17]. These variations in particle size are critical for assessing the environmental and health impacts of brake emissions since smaller particles are more likely to penetrate deep into the respiratory system [10][18].

The material composition of brake pads and rotors is another major determinant of brake emissions [11] [17][20][21]. Different formulations—such as low metallic (LM), semi-metallic (SM), and non-asbestos organic (NAO) linings—exhibit varying wear characteristics under identical braking conditions. Low metallic pads, for instance, produce higher emissions due to their abrasive contents, while NAO pads generate fewer particles but are less effective at high temperatures [20][21]. The interaction between pad material and rotor composition also affects the chemical composition of emitted particles. Studies consistently report that iron (Fe), copper (Cu), barium (Ba), and zinc (Zn) dominate the elemental makeup of brake wear debris, with Fe primarily originating from rotor wear [17][18] [21]. These chemical signatures are not only crucial for identifying the source of emissions in environmental monitoring, but also for understanding the mechanisms driving particle generation under different thermal and mechanical stresses.

Temperature sensitivity is another critical factor influencing brake emissions [16][22][23]. As disc temperatures rise during prolonged or aggressive braking events, the rate of particle generation increases significantly due to enhanced frictional wear and thermal decomposition of organic binders in brake linings. Laboratory dynamometer tests have demonstrated that airborne PM fractions can constitute up to 70% of total wear debris at moderate temperatures (100–200°C), but this proportion decreases at higher temperatures as larger particles dominate mass-weighted size distributions [16][22]. This temperature-dependent behavior highlights the importance of including thermal effects in brake emission models to accurately predict particle size distributions and emission factors under real-world conditions.

In addition, to model these complex interactions effectively, researchers have employed a combination of real-world data collection and controlled laboratory testing [9][11][14][16][22]. Real-world driving data from harmonized test cycles (e.g., WLTP or WLTC) provide statistically representative inputs for vehicle speed profiles, deceleration phases, and trip durations across diverse traffic conditions [15]. Laboratory dynamometer systems equipped with dilution tunnels enable precise measurement of mass emission factors, particle size distributions, and chemical composition under controlled conditions that replicate real-world airflow and thermal effects [16][22]. Advanced analytical tools such as Electrical Low-Pressure Impactors (ELPI) and Micro-Orifice Uniform Deposit Impactors (MOUDI) are used to capture real-time particle size distributions while isolating brake wear emissions from other sources like road dust or tire wear [12][15].

In summary, a robust brake emission model must integrate key contributors such as energy dissipation metrics, material properties of brake components, temperature

sensitivity, and real-world operational parameters. The conversion of kinetic energy into thermal energy during braking serves as a fundamental driver of PM generation, influencing both wear rates and particle characteristics. Material composition determines emission factors and chemical signatures, while temperature effects shape particle size distributions across different braking scenarios. By combining real-world driving data with laboratory-based validation methods, researchers can develop comprehensive models that accurately reflect the dynamics of brake wear emissions under diverse conditions. Such models are essential for informing regulatory policies aimed at mitigating non-tailpipe particulate matter emissions from vehicles.

Methodology

This section outlines the methods and processes employed to develop a robust framework for estimating brake emissions using advanced roadside sensors (e.g., LiDAR, camera) or remoting sensing technology, and hybrid physical-machine learning models. The methodology is designed to integrate multi-source and multi-modal sensor data with advanced modeling techniques to detect vehicles (including localization, classification), refine their trajectories (with multi-object tracking), identify braking events, and estimate non-tailpipe particulate emissions. Each component of the system is carefully calibrated and validated to ensure accuracy and scalability under diverse traffic conditions. The subsequent sections describe the system architecture, data processing workflows, model development procedures, and validation strategies in detail.

System architecture

The proposed system architecture, as shown in Figure 4, provides a comprehensive framework for estimating brake emissions using roadside LiDAR data and hybrid physical machine learning models. The system is divided into two main chains: the *Application Loop* on the left and the *Model Development* on the right, separated by a dashed line. The architecture is color-coded for clarity: “green” blocks represent sensor inputs such as LiDAR, GPS, cameras, and OBDs; “blue” blocks represent models that process or analyze data; “orange” blocks represent datasets used for training, validation, or calibration; and “purple” blocks highlight the final system output—brake emissions.

The *Application Loop* processes data sequentially through multiple modules to estimate brake emissions. Firstly, roadside LiDAR sensors collect high-resolution point cloud data to detect vehicles, generate bounding boxes, classify detected objects, and localize them through a detection model. These bounding boxes are then passed to a trajectory refinement module that tracks each individual object, smooths noisy or imputes incomplete trajectories, and outputs refined trajectory features such as speed and acceleration for the respective object. The refined trajectories are then analyzed by a brake activity detection model to identify braking events and their associated characteristics such as brake duration and brake intensity. Finally, these outputs are fed into a brake emission estimation model that calculates particulate matter emissions generated during braking events.

The *Model Development* focuses on offline tasks to train, validate, and calibrate the models used in the *Application Loop*. The Validation Dataset includes trajectory data such as speed and acceleration from the trajectory refinement module paired with brake light status obtained from cameras. The Training Dataset is composed of trajectory data including speed and acceleration collected from GPS devices along with brake pressure information from OBD of the probe vehicle. The Brake Emission Dataset, derived from

existing research based on dynamometer tests in laboratory settings, provides empirical data for calibrating the brake emission estimation model.

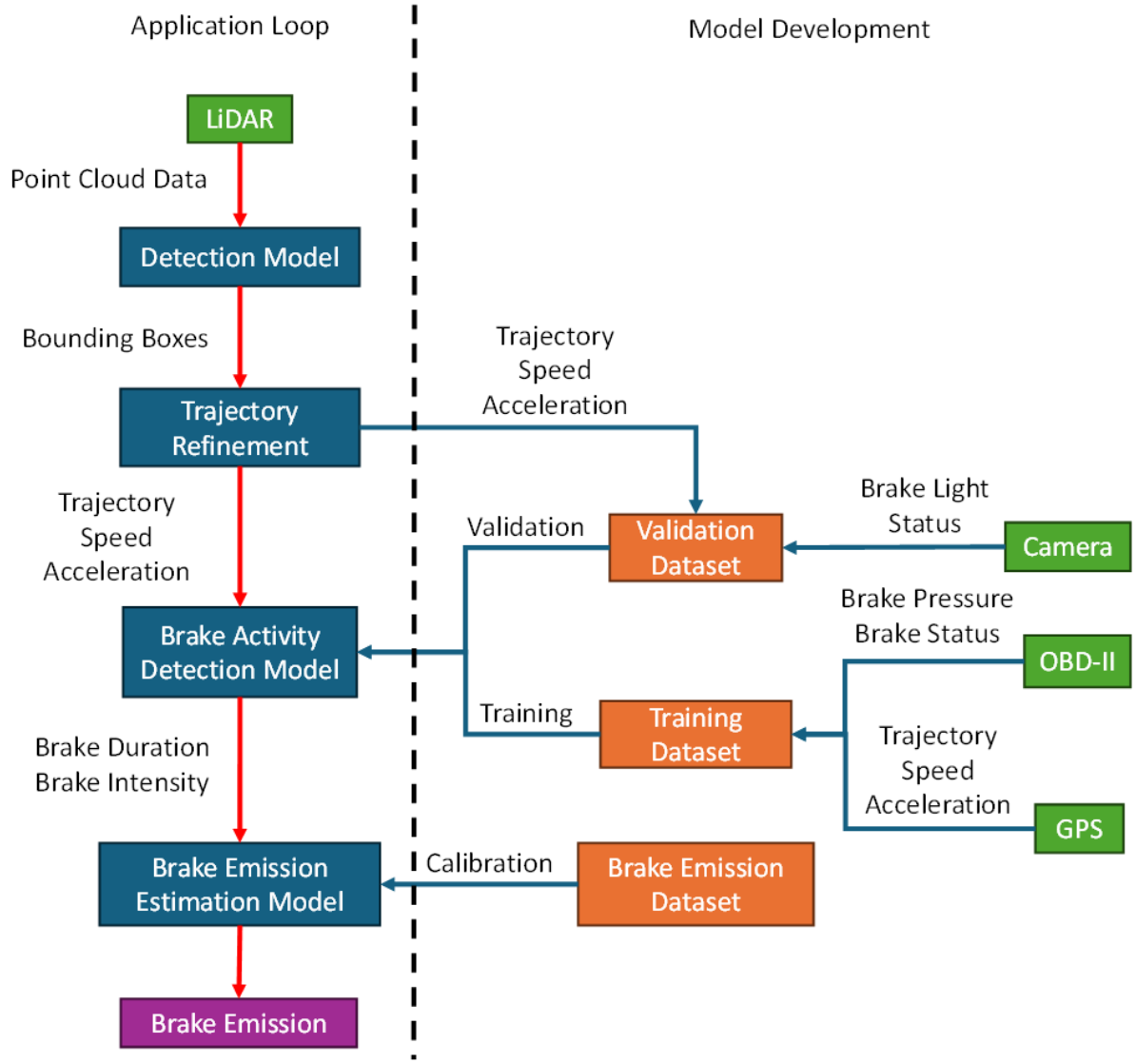

Figure 4. System architecture diagram.

This dual-loop design ensures that real-world operations in the *Application Loop* are supported by robust models continuously refined through offline development processes in the *Model Development*. By integrating high-resolution sensor data with advanced modeling techniques, this system delivers precise estimates of non-tailpipe emissions under diverse traffic conditions. The following sections will elaborate the details of each key component as illustrated in Figure 4.

LiDAR-based vehicle detection

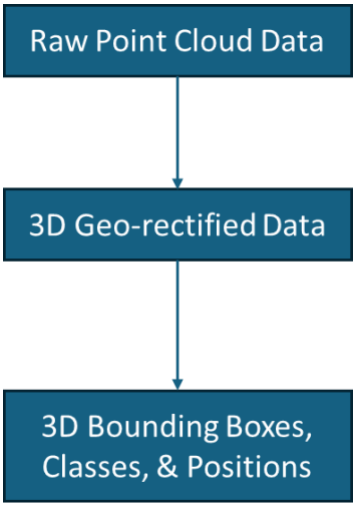

Figure 5. Workflow of LiDAR vehicle detection.

The vehicle detection process is a critical component of the system, as it identifies vehicles from high-resolution point cloud data collected by roadside LiDAR sensors (in this study). As shown in Figure 5, the detection pipeline consists of three main steps: 1) raw point cloud data collection, 2) coordinate transformation, and 3) PointPillar-based detection. Each step is designed to ensure the accurate generation of 3D bounding boxes that serve as inputs for subsequent modules in the system architecture.

The process begins with raw LiDAR data collected at a frequency of 10 Hz. This data provides detailed spatial information about objects within the sensor's field of view, including their positions and reflectivity. However, because the pre-trained nuScenes detection model was designed for onboard LiDAR sensors mounted on moving vehicles, a critical transformation of coordinates and rotation is required to adapt the model for use with stationary roadside LiDAR sensors. The transformation aligns the fixed roadside coordinate system with the global reference frame assumed by the detection model.

The coordinate transformation involves both rotational and translational adjustments using homogeneous transformation matrices. The rotational component accounts for pitch, yaw, and roll angles of the LiDAR relative to a standard Cartesian coordinate system, ensuring that the orientation of the point cloud aligns with the global reference frame. The translational component corrects for offsets between the physical location of the LiDAR sensor on a signal pole and its designated origin point in the roadside coordinate system. Mathematically, this transformation is represented as:

$$P_{transformed} = T \cdot P_{raw}$$

where P_{raw} represents raw point cloud data in the local LiDAR coordinate system, T is the transformation matrix combining rotation and translation, and $P_{transformed}$ is the

transformed point cloud data aligned with the global reference frame. This alignment ensures that all detected objects are positioned consistently within a shared spatial reference, enabling accurate downstream processing.

After applying this transformation, the processed 3D point cloud data is passed to a pre-trained MMDet3D detection model based on PointPillars. PointPillars was chosen for its ability to efficiently process large-scale point cloud data while maintaining high accuracy in detecting objects. The model generates 3D bounding boxes for each detected vehicle, including their position, orientation, and dimensions. These bounding boxes serve as inputs for subsequent modules such as trajectory refinement and brake activity detection.

As illustrated in Figure 5, this pipeline ensures that raw LiDAR data is effectively transformed and processed into 3D bounding boxes.

Trajectory refinement

The trajectory refinement process is a critical step in the system architecture, as it transforms raw bounding box detections into smooth, continuous trajectories that include accurate position, speed, and acceleration information. This step addresses issues such as noisy detection, missed frames, and inconsistencies caused by occlusions or sensor limitations. As shown in Figure 6, the trajectory refinement pipeline consists of several key stages: 1) confidence-based filtering, 2) lane-based geo-fencing, 3) multi-object tracking, 4) extraction of discontinuous trajectories, 5) interpolation, and 6) vector-based projection of acceleration.

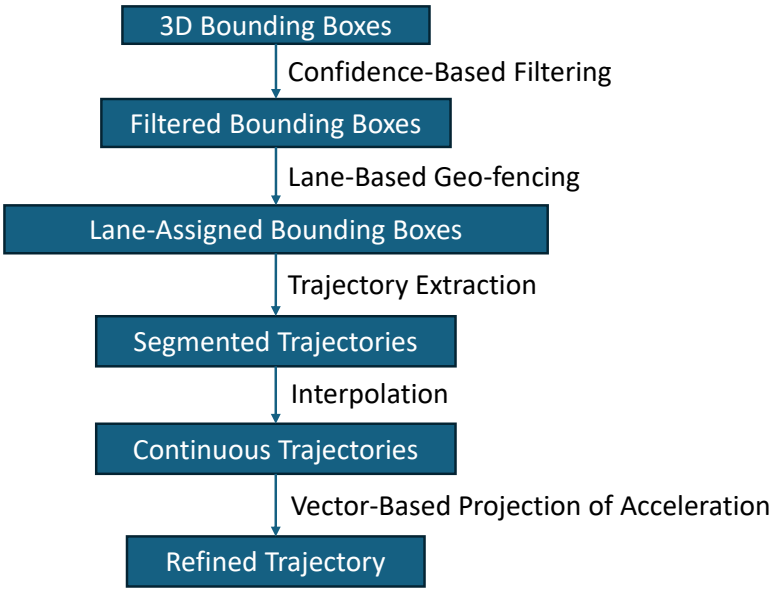

Figure 6. Workflow of trajectory refinement.

The process begins with *confidence-based filtering*. Bounding boxes generated by the detection model are assigned confidence scores that indicate the likelihood of valid detection. A threshold score (0.3 in this study) is applied to retain only bounding boxes with sufficient confidence. This step eliminates low-quality detections that could introduce noises into the tracking and refinement processes. The filtered bounding boxes are then passed over to the next stage for spatial assignment.

Lane-based geo-fencing is applied to separate bounding boxes based on their locations within predefined lane boundaries (according to the map information) in the LiDAR coverage area. The geo-fencing process uses the known geometry of the road and intersection to assign each bounding box to a specific lane. This step assumes that vehicles do not change lanes when approaching an intersection near solid lane markings, which is generally a reasonable assumption in the real-world driving. By associating bounding boxes with specific lanes, geo-fencing reduces ambiguities caused by overlapping objects and improves the performance of the tracking algorithm, thus better trajectory generation.

After geo-fencing, multi-object tracking is performed using *AB3DMOT*, an algorithm designed for 3D object tracking in dynamic environments. Basically, AB3DMOT assigns unique IDs to detected vehicles and links their positions across consecutive frames based on spatial and temporal consistency. The algorithm uses a combination of motion models and an Intersection over Union (IoU)-based matching strategy to maintain object identities over time. For this system, AB3DMOT is configured with the following parameters: 1) a maximum age of 5 frames to handle temporary occlusions, 2) a minimum hit count of 3 to confirm valid tracks, and 3) an IoU threshold of 0.3 for associating detections with existing tracks. These settings balance robustness against occlusions and sensitivity to new objects entering the field of view.

Once tracking is complete, segmented trajectories are extracted for further processing. These trajectories consist of position, speed, and acceleration data in the x, y, and z directions, but may contain gaps or inconsistencies due to missed detections or occlusions, as well as variable scanning frequency which AB3DMOT does not account for. To address these issues, firstly, a custom Kalman filter is created to handle variable timesteps between LiDAR frames. Explicit timesteps are stored and complete position and velocity history for each tracked object is maintained using a 10x10 state transition matrix (including position, orientation, dimensions, and velocity). Additional smoothing is also performed with automatic uncertainty balancing covariance initialization (high initial velocity uncertainty, low process noise) and dynamic propagation mechanisms. The transition matrix adjusts uncertainty proportionally to measurement gaps. Interpolation and ID merging are then performed on the trajectories taken from the custom Kalman filter. Data is interpolated at a uniform time interval of 0.1 seconds. The interpolation process reconstructs missing portions of the trajectory by fitting cubic splines or other interpolation functions to the available data points. This step ensures that each trajectory is smooth and continuous, with consistent temporal resolution.

After interpolation, an average window taking the 5 closest data points to smooth fluctuations due to noise. Finally, vector-based calculations are performed to refine speed and acceleration values further. The vector sum of speed components in the x, y, and z directions is computed to obtain the total speed magnitude for each time step:

$$v_{total} = \sqrt{v_x^2 + v_y^2 + v_z^2}$$

Similarly, acceleration components are summed to calculate the total acceleration magnitude:

$$a_{total} = \sqrt{a_x^2 + a_y^2 + a_z^2}$$

The acceleration vector is then projected onto the direction of the longitudinal direction vector to determine the effective acceleration along the longitudinal direction:

$$a_{projected} = \vec{a} \cdot \vec{l}$$

$$v_{projected} = \vec{v} \cdot \vec{l}$$

where $\vec{a}$ represents the acceleration vector and $\vec{l}$ represents a unit vector with a magnitude of 1 that points in the direction of the lane leading toward the intersection. This projection ensures that acceleration values are consistent with the vehicle's actual movement dynamics.

As illustrated in Figure 6, this pipeline transforms raw bounding box detections into refined trajectories that include accurate position, total speed, total acceleration, and effective acceleration along the motion direction. These refined trajectories serve as inputs for downstream modules such as Brake Activity Detection and Brake Emission Estimation, enabling precise analysis of braking events and associated emissions under real-world traffic conditions.

Development of the brake activity detection model

The Brake Activity Detection Model integrates physical principles of vehicle dynamics with data-driven techniques to identify and characterize braking events. The model predicts two critical outputs: 1) the occurrence of braking events, and 2) the corresponding brake intensity. These predictions are achieved by decomposing the total acceleration of a vehicle into its constituent components, each representing a specific physical force acting on the vehicle. This decomposition ensures that the model is both interpretable and adaptable to real-world complexities, such as heterogeneous vehicle types, varying road conditions, and driver behavior. As shown in Figure 7, the workflow for developing this model involves initializing physical parameters, computing predicted total acceleration, calculating a loss function, updating parameters iteratively, and validating the trained model.

The workflow begins with the initialization of physical parameters that define the proportional relationship between specific forces acting on a vehicle. These parameters include coefficients for crawling acceleration $k_{crawling}$, rolling resistance $k_{rolling}$, aerodynamic drag k_{air}, road gradient k_{road}, and braking acceleration k_{brake}. These initial values are either derived from empirical studies or set to reasonable starting points based on the prior knowledge of vehicle dynamics.

Using these parameters, the model calculates the predicted total acceleration a_{total} for each sample in the training dataset. The total acceleration is expressed as:

$$a_{total} = a_{crawling} + a_{rolling} + a_{air} + a_{road} + a_{brake}$$

Each term in this equation corresponds to a specific physical phenomenon. The crawling acceleration $a_{crawling}$ represents the positive acceleration observed at very low speeds when the vehicle starts moving forward after releasing the brake pedal. This phenomenon, often referred to as "crawling," occurs in automatic transmission vehicles and diminishes rapidly as speed increases. It is modeled as:

$$a_{crawling} = k_{crawling} * \max\left(-\log\left(\max\left(v, 0.1\right)\right) + 1{,}0\right)$$

where, $k_{crawling}$ is a proportionality constant learned during training, and v represents the vehicle's velocity. The logarithmic dependence on velocity reflects how crawling effects are significant only at very low speeds and diminish quickly as speed increases. The clamping operation ensures that $a_{crawling}$ remains physically valid for all velocity values.

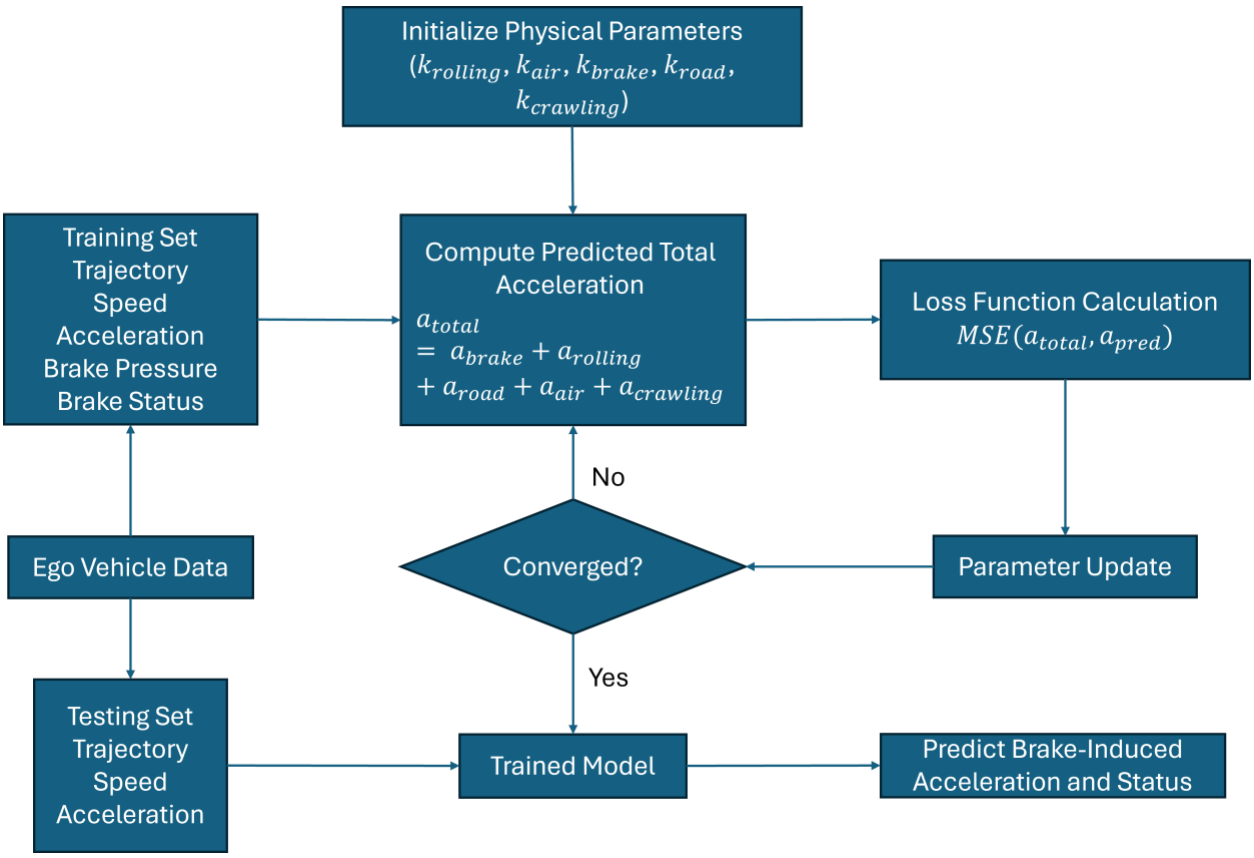

Figure 7. Workflow of brake activity detection model.

Rolling resistance $a_{rolling}$ accounts for energy losses due to tire deformation and road surface interactions. It is modeled as:

$$a_{rolling} = -k_{rolling} * g$$

where, $k_{rolling}$ is a dimensionless coefficient representing rolling resistance, and g is the gravity acceleration. This term remains constant across different speeds but varies with factors such as tire composition, inflation pressure, and road surface conditions.

Aerodynamic drag a_{air} represents the resistance exerted by air on the moving vehicle. It increases quadratically with velocity and is given by:

$$a_{air} = -k_{air} * v^2$$

The parameter k_{air} encapsulates factors such as the vehicle's frontal area, drag coefficient, and air density. This term becomes especially significant at higher speeds, where aerodynamic drag dominates other resistive forces.

Road gradient resistance a_{road} captures the influence of road inclination on acceleration or deceleration. It is expressed as:

$$a_{road} = -k_{road} * g$$

The parameter k_{road} represents the sine of the road gradient angle and determines whether gravity contributes to acceleration (downhill) or deceleration (uphill).

Finally, braking-induced deceleration a_{brake} is directly proportional to brake pressure and is modeled as:

$$a_{brake} = -k_{brake} * pressure$$

In this equation, k_{brake} represents the braking system's efficiency in converting hydraulic pressure into deceleration. Brake pressure data obtained from onboard sensors in the data collection and is fed into training process. After training, a_{brake} will be estimated in the testing and the application loop.

These components are combined into a differentiable physics model that computes total acceleration as a function of speed, brake pressure, and learned parameters $k_{crawling}$, $k_{rolling}$, k_{air}, k_{road}, and k_{brake}. This formulation enables gradient-based optimization during training.

The training process involves optimizing these five parameters using real-world trajectory data collected from the probe vehicle during braking events. The dataset includes time-series measurements of speed, distance to the intersection, acceleration, brake pressure, and brake status.

The predicted total acceleration is compared against observed acceleration values from real-world trajectory data to calculate a loss function. The Mean Squared Error (MSE) loss function measures the difference between predicted acceleration, a_{pred}, and observed acceleration, $a_{measured}$:

$$L = \frac{1}{N}\sum_{i=1}^{N}\left(a_{pred,i} - a_{measured,i}\right)^2$$

This loss is minimized iteratively using gradient-based optimization techniques such as *Adam* [24]. During each iteration, parameters are updated to reduce prediction errors while ensuring physical validity through constraints such as non-negativity. The Adam optimizer is employed to update parameters iteratively over 50 epochs.

As shown in Figure 7, this iterative process continues until convergence is achieved—when further updates result in negligible improvements in model performance. Once trained, the model isolates braking-induced deceleration by subtracting other components from total measured acceleration:

$$a_{brake,pred} = a_{measured} - (a_{crawling} + a_{rolling} + a_{air} + a_{road})$$

After training, the model can estimate brake pressure from predicted accelerations and identify braking events across diverse traffic scenarios. By combining physically interpretable components with machine learning techniques, this hybrid framework

bridges theoretical modeling with practical applications in traffic monitoring and environmental impact assessment.

Model validation

The model validation (including the dataset generation) is a critical component of the system architecture, as it ensures the Brake Activity Detection Model performs reliably under real-world conditions. As shown in Figure 4, the validation dataset is derived from two primary sources: 1) trajectory data (speed and acceleration) generated by the Trajectory Refinement module, and 2) manually labeled brake light status timestamps obtained from video footage captured by stationary cameras. This dataset does not include brake pressure or brake intensity due to the absence of OBD data in the validation process, which limits direct comparisons of deceleration magnitudes. Instead, the validation focuses on evaluating the model's ability to detect braking events based on brake light activations.

To construct the validation dataset, brake light activations are manually labeled using video footage recorded by stationary cameras positioned at key locations near intersections. These cameras are configured to capture clear views of vehicles' rear ends under low-light conditions during evening hours when brake lights are most visible. Trained annotators review each video frame-by-frame to identify instances where brake lights are illuminated. This manual labeling process ensures high accuracy in associating brake light activations with specific vehicles detected by LiDAR. Although computer vision algorithms could potentially automate this task in future implementations, manual labeling was chosen for this proof-of-concept study due to its reliability and precision.

The labeled brake light data is synchronized with LiDAR-detected trajectories based on timestamps extracted from both datasets. This synchronization ensures that each trajectory includes accurate information about whether braking occurs during any given time interval. The synchronized dataset combines trajectory features such as speed and acceleration with binary brake light status (on/off) for each time step.

Since the validation dataset lacks direct measurements of brake pressure or intensity, evaluating the Brake Activity Detection Model requires alternative performance metrics. One key metric is confusion matrix, which measures how well the model's predicted braking events align with observed brake light activations in the validation dataset. Confusion matrix is defined as:

$$Confusion\ Matrix = \begin{matrix} TN & FP \\ FN & TP \end{matrix}$$

A high confusion matrix indicates that the model successfully detects most braking events identified by manual labeling. However, it is important to note that confusion matrix alone does not capture false positives—instances where the model predicts braking events that

do not correspond to observed brake light activations. To address this limitation, additional metrics such as *precision* and *recall* can be calculated:

$$Precision = \frac{True\ Positives\ (TP)}{True\ Positives\ (TP) + False\ Positives\ (FP)}$$

Precision evaluates the proportion of predicted braking events that correspond to actual brake light activations.

$$Recall = \frac{True\ Positives\ (TP)}{True\ Positives\ (TP) + False\ Negative\ (FN)}$$

Recall assesses the proportion of observed brake light activations that are correctly identified by the model.

These metrics provide a comprehensive assessment of the model's performance in detecting braking events under real-world conditions.

The absence of brake pressure or intensity data in the validation dataset means that direct comparisons of deceleration magnitudes are not possible. Instead, the focus shifts to evaluating whether the model accurately identifies braking events based on binary indicators such as brake light status. While this limitation restricts certain types of analysis, it also highlights opportunities for future work, such as incorporating additional data sources like OBD inputs or using advanced computer vision techniques to infer deceleration magnitudes from visual cues.

By leveraging high-quality manual annotations and synchronized trajectory data, the validation dataset provides a robust foundation for assessing the Brake Activity Detection Model's performance. The insights gained from this process contribute to refining the model and ensuring its applicability across diverse traffic scenarios.

Development and calibration of brake emissions estimation model

The estimation of non-tailpipe emissions from braking events is a critical component of this study, as it quantifies particulate matter generated due to the dissipation of kinetic energy during braking. According to existing research, a proportional relationship has been established between the energy dissipated during braking and the amount of particulate matter emitted [14][23]. This insight forms the foundation for the physics-based model used in this study, which integrates vehicle dynamics with traffic data collected through roadside sensors to compute brake-induced emissions with high temporal and spatial accuracy.

The total brake-induced particulate emissions are calculated using the following equation:

$$E_{PM} = k * KE = \frac{1}{2} kmv^2$$

where KE is kinetic energy, the coefficient k is an empirical emission factor that translates the energy dissipated during braking into particulate matter emissions. This factor is calibrated using existing data from laboratory studies or field measurements and accounts for variables such as brake pad material, brake pad temperature, and environmental conditions. The velocity v (in m/s) is the instantaneous speed of the vehicle, while m (in kg) is the estimated vehicle mass derived from LiDAR-detected vehicle class (or bounding box dimensions). Note that

$$\frac{d(E_{PM})}{dt} = \frac{d(k * KE)}{dt} = kmv * (\frac{dv}{dt}) = kmva$$

Therefore,

$$E_{PM} = k \cdot \sum(v(t) \cdot m \cdot a_{brake}(t) \cdot \Delta t)$$

In this equation, E_{PM} represents the total PM emissions (e.g., in micrograms) generated over a given time period. The term a_{brake} (in m/s^2) represents the deceleration due to braking, as predicted by the hybrid physical-machine learning model. Finally, Δt (in s) is the time interval over which emissions are aggregated.

To compute brake wear emissions for individual vehicles, the methodology follows two sequential steps. First, the vehicle trajectory data (velocity, acceleration, and estimated mass) is processed through the brake activity detection model to isolate braking-specific deceleration $a_{brake}(t)$ at each time step. Second, $E_{PM} = k \cdot \sum(v(t) \cdot m \cdot a_{brake}(t) \cdot \Delta t)$ is applied by summing the product of $v(t), m, a_{brake}(t)$ and Δt (0.1s) across all braking instances in the trajectory, scaled by the material-specific emission factor k.

The empirical emission factor k plays a critical role in this framework and is derived from existing studies on brake wear emissions conducted under controlled conditions, such as dynamometer tests. The vehicle mass m is estimated based on the size of the bounding box detected by LiDAR sensors, and the classification aligns with the nominal weight factors suggested by the EPA MOVES model [25]. The dimensions of each bounding box—length, width, and height—are used to classify vehicles into categories such as passenger cars, light-duty trucks, or heavy-duty vehicles. Each category is assigned a representative mass based on its Gross Vehicle Weight Rating (GVWR) as defined by MOVES. For instance, passenger cars are assigned a nominal weight of 1,500 kg, light-duty trucks are assigned 2,500 kg, and heavy-duty trucks are assigned 10,000 kg. These nominal weight factors ensure that mass estimates are consistent with real-world vehicle distributions and regulatory standards. By adhering to EPA MOVES classifications, this approach provides a standardized method for estimating vehicle mass while maintaining compatibility with emissions modeling frameworks.

The velocity v and deceleration due to braking a_{brake} are obtained directly from the interpolated trajectory data processed through the brake activity detection model. The velocity represents the instantaneous speed of each vehicle at a given time step, while a_{brake} isolates the component of total deceleration attributable specifically to braking forces. This separation ensures that only braking-related energy dissipation contributes to emission calculations.

The temporal resolution Δt corresponds to the time interval between consecutive data points in the interpolated trajectory data used as input for brake activity detection. For example, if interpolation generates data at uniform intervals of 0.1 seconds, then $\Delta t = 0.1$ seconds. This approach ensures that emissions are calculated with high temporal precision while aligning with the resolution of input data.

The calibration of the empirical emission factor k is a critical step in ensuring that the brake emission estimation model accurately reflects real-world conditions. The factor k encapsulates the proportional relationship between energy dissipated during braking and particulate matter emissions, as established by existing studies conducted under controlled conditions such as dynamometer tests. To calibrate k, a regression-based approach is employed using empirical data from these studies [26]. The calibration dataset includes measurements of brake wear emissions under varying conditions of brake pressure, temperature, and vehicle speed.

The regression process involves fitting a model that relates the observed brake wear emissions to the estimated total brake emission.

$$L = \sum_{i=1}^{N} (E_{Observed-PM} - E_{Predicted-PM})^2$$

where:
L is the total loss over all samples in the calibration dataset,
N is the number of samples,
k is iteratively adjusted to minimize L.

The regression assumes a linear relationship between energy dissipation and particulate matter emissions, as supported by existing research. The calibrated value of k represents this proportional relationship and accounts for variations in vehicle types, road conditions, and other environmental factors.

This methodology allows instantaneous estimation of brake wear emissions for individual vehicles detected by LiDAR. By summing up all time steps within a given braking event for a single vehicle, it is possible to calculate total emissions generated during that specific event. This capability enables detailed analyses of non-tailpipe emissions at both individual vehicle and population levels across various traffic scenarios.

The use of LiDAR-based trajectories ensures that this framework captures real-world driving behaviors and braking patterns rather than relying on laboratory simulations or static assumptions about traffic flow. High-frequency sensor data allows for fine temporal granularity in emission estimates, enabling detailed analyses of transient events such as sudden braking or stop-and-go traffic conditions.

This approach provides significant advantages over traditional methods for estimating non-tailpipe emissions by leveraging advanced sensing technologies and physics-based modeling techniques. The results will contribute to improving non-tailpipe emission inventories by providing accurate estimates of brake wear contributions under real-world conditions. These findings will inform regulatory efforts aimed at mitigating non-tailpipe particulate matter pollution and addressing these issues in low-income communities disproportionately affected by near-road pollution.

Case Study

To evaluate the proposed methodology, the research team conducted a case study at the intersection of University Ave. and Iowa Ave. in Riverside, California (see the Google Map image in Figure 8).

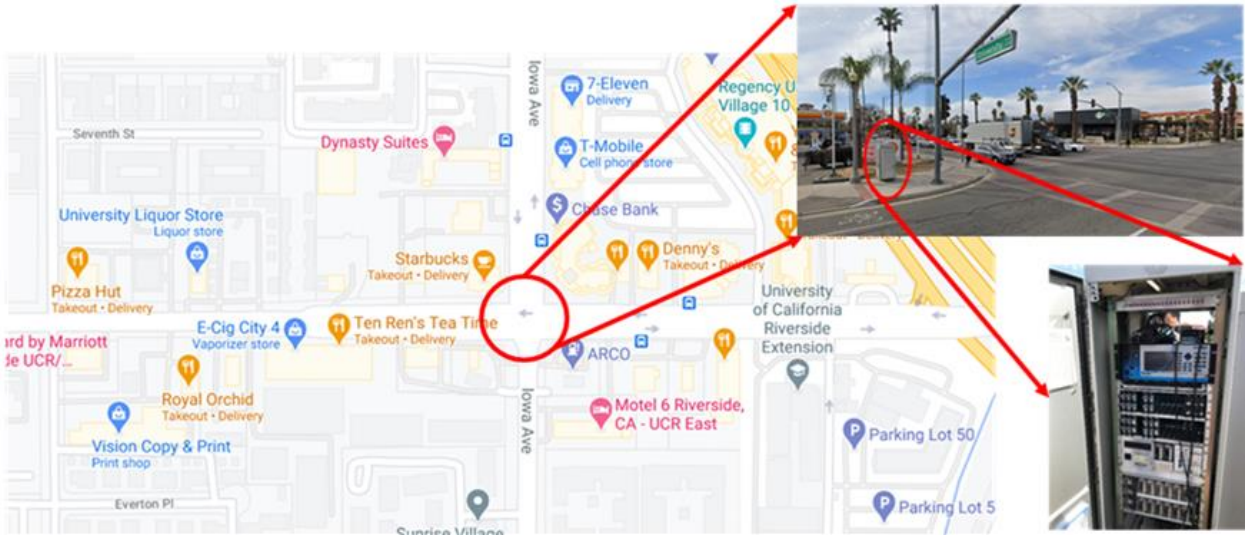

Figure 8. Test site at the intersection of University Ave. and Iowa Ave. in Riverside, CA.

Data collection

The data collection process for this study was meticulously designed to capture real-world braking activities and traffic dynamics at a real-world intersection (specifically, University Ave. and Iowa Avenue in Riverside, CA in this study). This location was selected due to its relevance to disadvantaged communities and its suitability for studying non-tailpipe emissions, particularly brake wear. The primary focus of this effort was to record braking activities as vehicles approached the intersection, leveraging advanced sensing technologies such as roadside LiDAR, drones, a portable roadside camera, and a probe vehicle equipped with multiple sensors (such as GPS logger and OBD-II). These tools were deployed strategically to ensure comprehensive coverage of the intersection and its approaches. Figure 9 provides an overview of the entire setup.

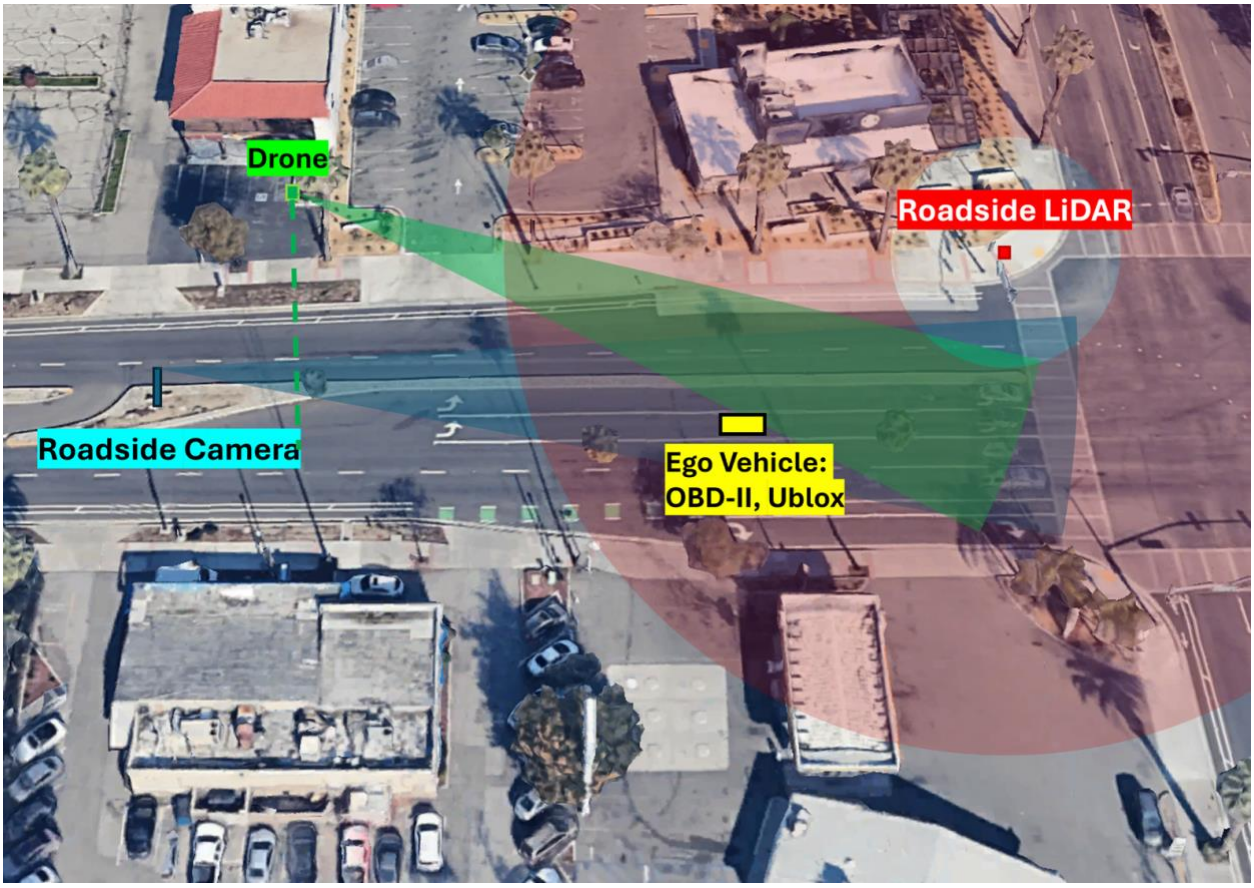

Figure 9. Data collection setup.

An OUSTER® OS1 64-Channel 3D LiDAR was installed at the northwest corner of the intersection, which is marked as a red circle in Figure 10. The LiDAR was mounted on a signal pole at a height of 14 to 15 feet above the ground. Its pitch and yaw angles were carefully calibrated to optimize coverage of the monitoring area, which is illustrated as an orange rectangle in Figure 10. The LiDAR provided high-resolution point cloud data that enabled vehicle object detection within its field of view. For effective detection, enough amount of point cloud data reflected from each vehicle was required, which limited reliable detection to vehicles located within approximately 40 meters of the sensor. At farther distances, sparse point cloud returns may be insufficient for robust object detection. The LiDAR system operated at a frame rate of 10 Hz, providing detailed temporal resolution for capturing vehicle movement dynamics within its effective range.

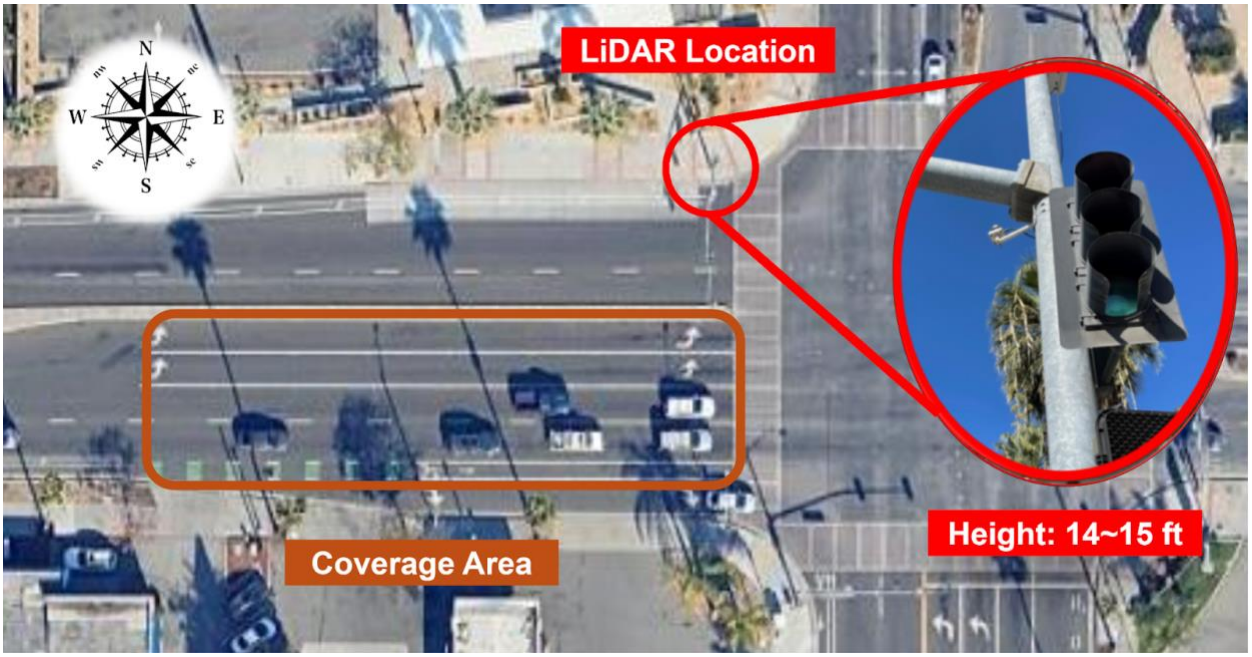

Figure 10. Roadside LiDAR setup.

To complement the roadside LiDAR, a DJI Mini 3 drone was deployed above the eastbound lanes approaching the intersection. The DJI Mini 3, as shown in Figure 11, is a lightweight drone weighing less than 249 grams, which makes it easy to deploy without requiring registration in most regions. The drone is equipped with a 1/1.3-inch CMOS sensor capable of capturing high-quality 4K HDR video at up to 60 frames per second and still images with a resolution of up to 48 megapixels. It features dual native ISO and an f/1.7 aperture, enabling excellent performance in low-light conditions. The drone has a maximum flight time of approximately 51 minutes under optimal conditions and a video transmission range of up to 10 kilometers using DJI O2 technology. For this study, the drone was flown at an altitude of approximately 45 meters, or 150 feet, providing an aerial perspective that captured macro-/mesoscopic traffic dynamics such as vehicle spacing, queue lengths, and driving behavior. Its flight path was specifically focused on eastbound traffic approaching the intersection to ensure that braking events were thoroughly documented. Equipped with high-definition cameras capable of recording in low-light conditions, the drone collected detailed video footage during data collection sessions. A sample clip view of the recorded drone footage is shown in Figure 12. The timing of data collection—around 6 PM when the sun had set—was deliberately chosen to enhance visibility of brake lights without interference from daylight glare. This approach ensured that braking events could be clearly identified from both aerial and ground perspectives.

Figure 11. DJI Mini 3.

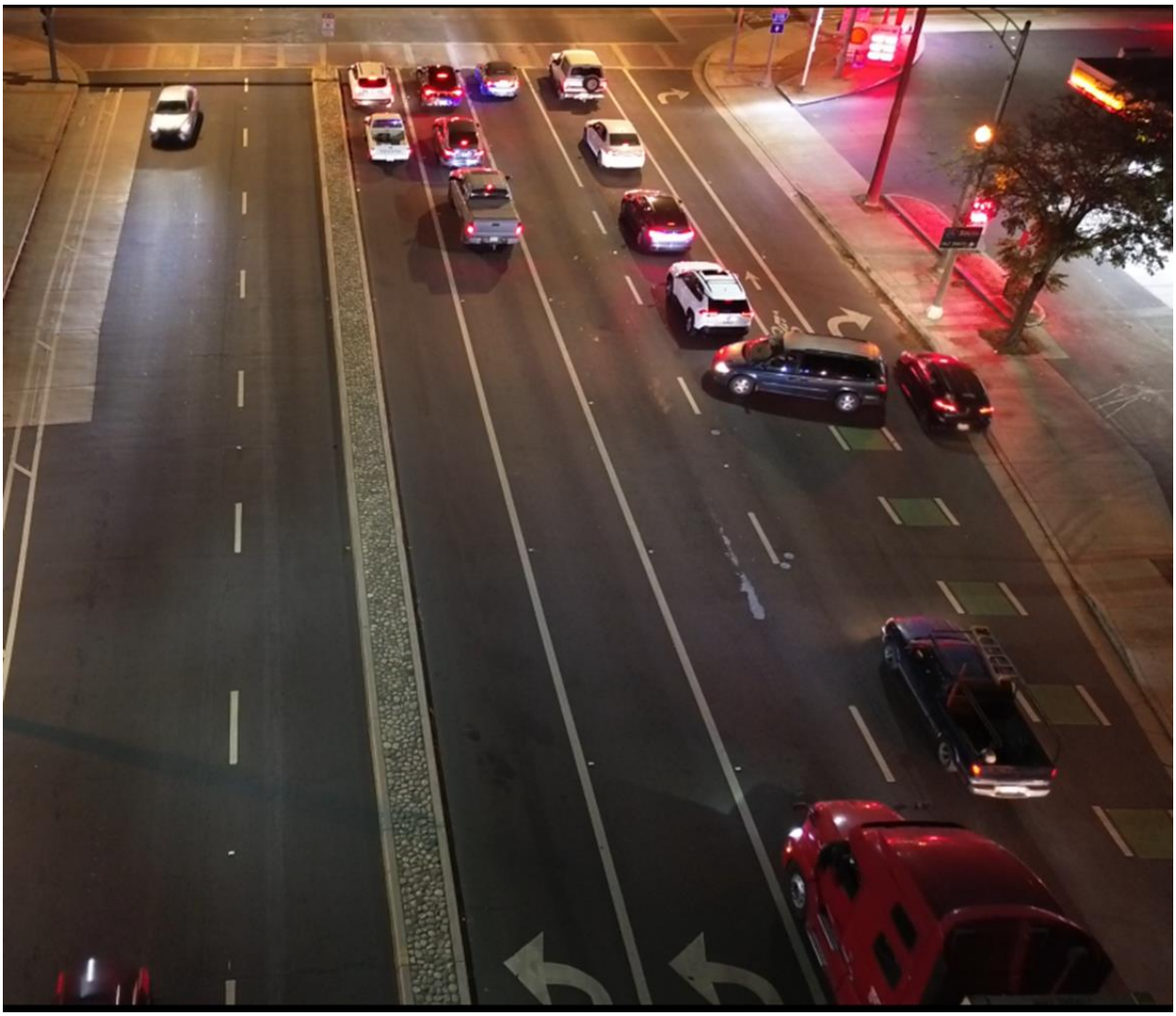

Figure 12. Sample clip view of recorded drone footage.

A portable roadside camera system was also deployed to capture braking events from ground level. This system consisted of a smartphone mounted on top of a tripod that stood approximately 2.5 meters tall. The tripod was portable and allowed flexible placement, depending on data collection needs. For this study, it was positioned on the median island along the eastbound approach to the intersection, which is a raised divider separating opposing lanes of traffic as vehicles approached the intersection. The camera faced eastward, directly observing vehicles as they approached the intersection. Its primary function was to detect brake light activations. By focusing on the rear of vehicles, this camera provided a clear view of brake lights, enabling accurate detection of braking events in terms of frequency and duration. While the camera may experience occlusion issues caused by other vehicles or objects blocking its view, the diffuse glow of brake lights recorded at night makes it possible to manually recognize brake light status. However, whether computer vision algorithms can reliably detect brake light activations under such conditions remains uncertain. Like the drone cameras, this roadside camera featured low-light imaging capabilities to ensure reliable performance during nighttime or twilight conditions. A sample clip from the roadside camera footage is shown in Figure 13, highlighting its ability to capture detailed braking activity at the same timestamp as the drone footage.

Figure 13. Sample clip view of roadside camera footage with the same timestamp as the drone footage.

The probe vehicle, a 2012 Toyota Corolla, was utilized for dynamic data collection within the study area as shown in Figure 14. It is a compact sedan powered by a 1.8-liter DOHC four-cylinder engine that delivers 132 horsepower and 128 lb-ft of torque. It features front-

wheel drive and achieves fuel efficiency ratings of approximately 26 miles per gallon in city driving and 34 miles per gallon on highways with its automatic transmission.

The probe vehicle was equipped with multiple sensors to support data collection efforts, including UBlox F9R GPS (Figure 15) and the CAN2USB device (Figure 16). The UBlox F9R GPS system provided highly accurate geolocation data with sub-meter precision, ensuring seamless alignment with spatial datasets collected by other systems such as LiDAR and cameras. In addition, the CAN2USB device was connected to the vehicle's OBD-II port to access real-time messages from the Controller Area Network (CAN). This device received raw CAN messages and sent them to a laptop inside the vehicle, where they were decoded and analyzed. The decoded messages enabled the extraction of critical vehicular performance metrics, including speed, acceleration, brake pressure, and brake on/off status. Together, these systems provided a comprehensive dataset for analyzing driver-specific responses to traffic conditions within the study area.

Figure 14. Probe vehicle.

Figure 15. UBlox F9R GPS in the probe vehicle.

Figure 16. CAN2USB device in the probe vehicle.

The data collection period was carefully chosen to ensure optimal conditions for capturing braking activity. Sessions were conducted around 6 PM, a time that enhanced visibility of brake lights under low-light conditions and coincided with peak traffic periods when braking events were more frequent due to congestion and signal changes. Weather conditions were monitored to avoid disruptions from rain or strong winds, although all sensors used in this study were designed to operate reliably under moderate

environmental variability. This timing and environmental consideration ensured the quality and consistency of the collected data.

The integration of data from multiple sources, including LiDAR, drones, roadside cameras, and a probe vehicle, resulted in a comprehensive dataset for analyzing brake activities. The LiDAR provided high-resolution spatial trajectories with a frame rate of 10 Hz, while the drone captured macro-level traffic dynamics such as vehicle spacing and queue lengths at up to 60 frames per second. The roadside camera focused on micro-level braking behaviors by detecting brake light activations at 30 frames per second, and the probe vehicle contributed to the ground truth information about vehicular states, such as speed, acceleration, and brake status, recorded at frequencies ranging from 1 to 10 Hz. These varied data rates ensured that both transient and sustained traffic behaviors were adequately captured.

After collection, the raw data underwent essential preprocessing steps to ensure quality and usability for further analysis. Outlier removal was applied to eliminate erroneous readings such as implausible acceleration values, and missing data points were addressed through imputation techniques. Each dataset was aligned using the timestamps recorded by the sensors, which allowed for matching data points from different sources based on their time of occurrence. This ensured that braking events captured by one sensor (e.g., the roadside camera) could be cross-referenced with corresponding vehicle trajectories, speeds, and other traffic dynamics from other sensors. This approach ensured that the diverse datasets could be effectively integrated into a cohesive framework for examining real-world braking activities and their implications for non-tailpipe emissions modeling.

LiDAR-based vehicle detection results

Figure 17 illustrates an example of detected 3D bounding boxes overlaid on the LiDAR point cloud data. The bounding boxes are color-coded to indicate different objects or confidence levels. This visualization highlights the system's capability to process complex traffic scenarios and provide precise spatial information about detected vehicles. The detection results demonstrate the system's ability to accurately identify vehicles in various traffic conditions. The raw LiDAR data is processed at a frequency of 10 Hz, and the PointPillars model ensures efficient detection while maintaining high accuracy. Confidence-based filtering is applied to retain only high-quality detections, reducing false positives and ensuring robustness of downstream modules.

Trajectory refinement results

Figure 18 illustrates an example of trajectory refinement result. The bounding boxes are restricted to a specific lane based on their spatial location within predefined boundaries. Each tracked vehicle is assigned a unique ID to maintain continuity across frames, as shown in the figure. After geo-fencing and tracking, trajectory refinement continues with

interpolation to address gaps in the data caused by missed detections or occlusions. Figure 19 provides a complete trajectory of a representative (detected) vehicle with refined position, velocity, and acceleration in the x, y, and z directions over time. The top panel (Figure 19 (a)) shows the raw position data in three dimensions (x, y, z), highlighting the initial noisy nature of the detections. The middle panel (Figure 19 (b)) illustrates the computed velocity components (v_x, v_y, v_z), which exhibit fluctuations due to inconsistencies in raw data. The bottom panel (Figure 19 (c)) displays the computed acceleration components (a_x, a_y, a_z), showing significant noise and variability in the raw data.

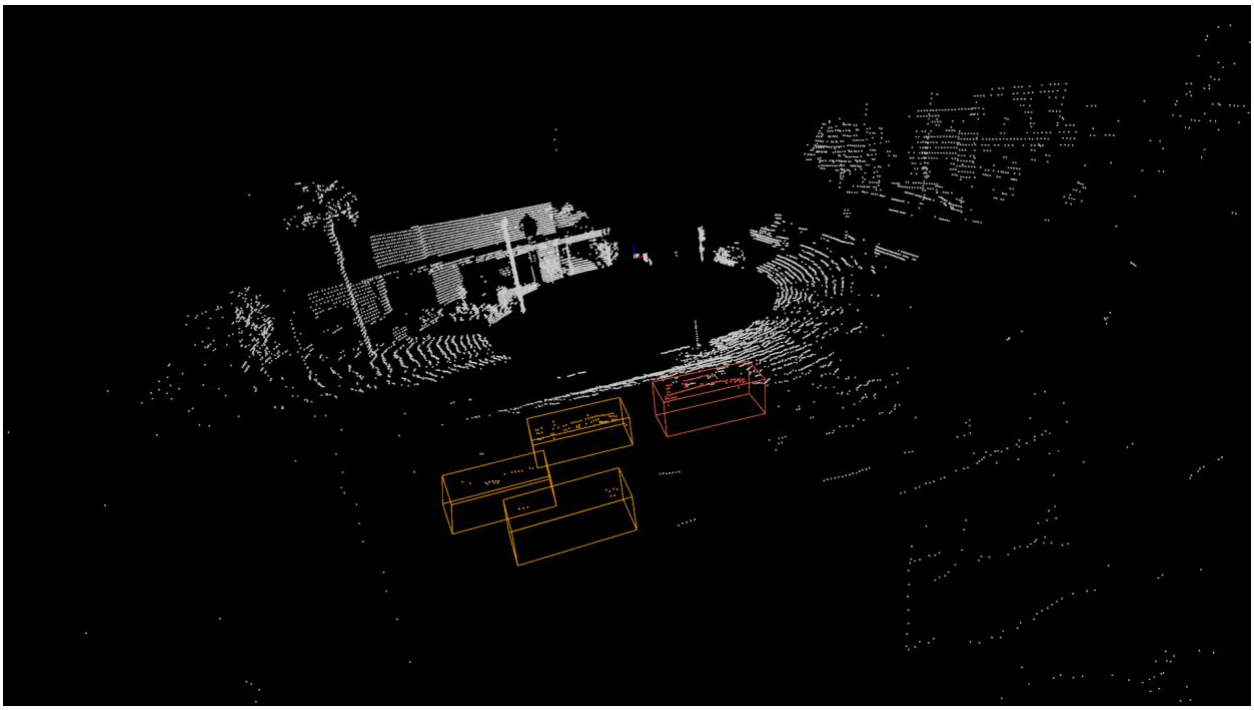

Figure 17. Detected 3D bounding boxes overlaid on LiDAR point cloud data.

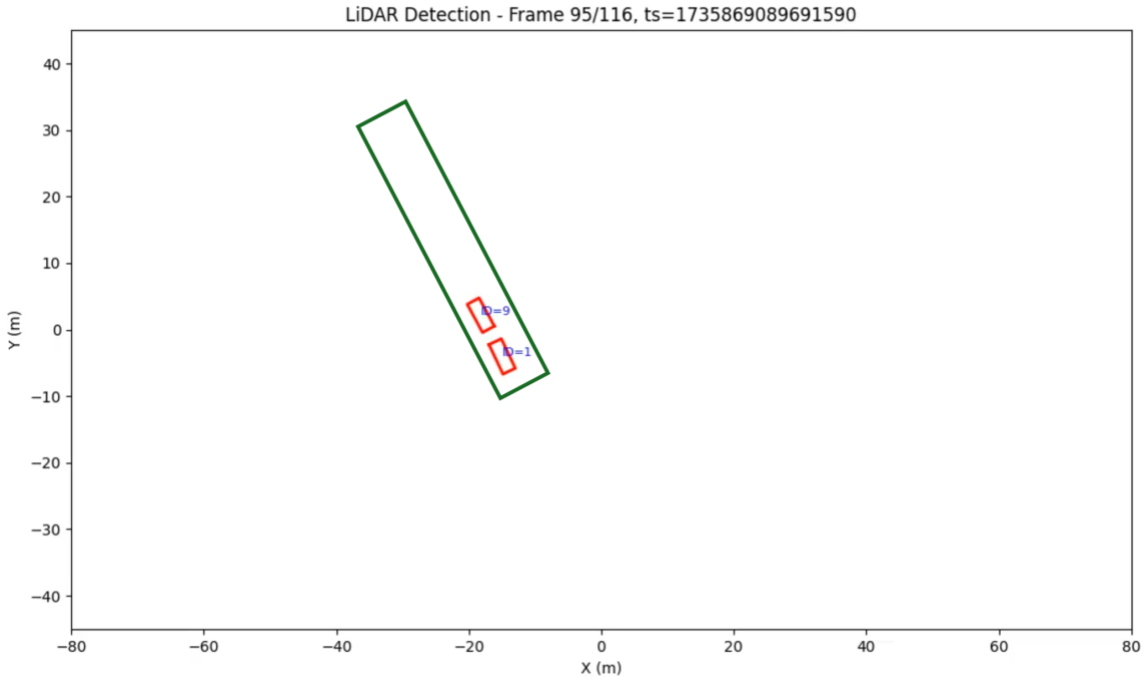

Figure 18. Geo-fenced bounding boxes with unique IDs assigned after tracking.

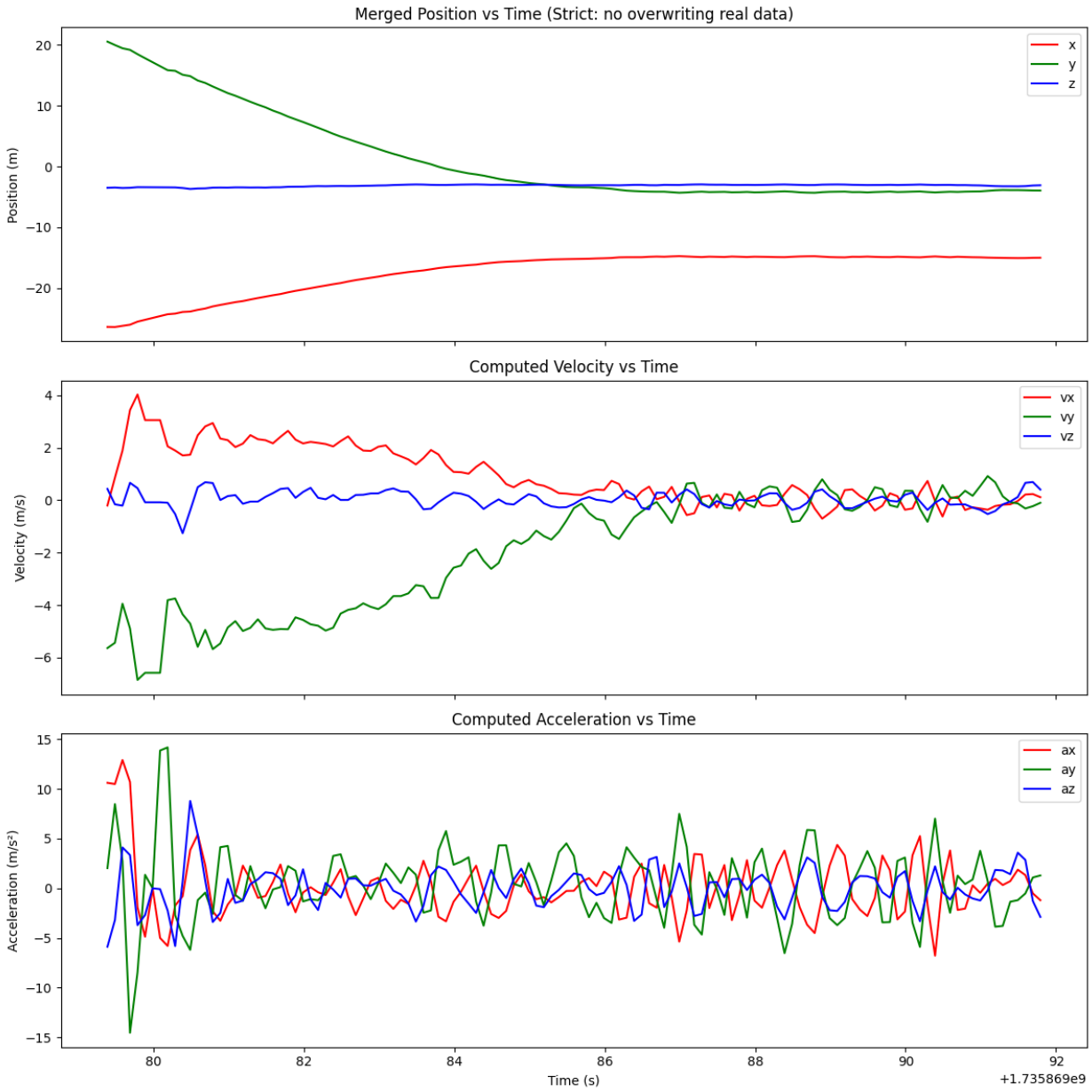

Figure 19. (A) refined position, (b) refined velocity, and (c) refined acceleration over time for a representative vehicle trajectory after interpolation.

The final stage of trajectory refinement involves applying vector-based projection techniques to compute smoothed trajectory features in terms of magnitudes. Figure 20 demonstrates these results by presenting smoothed position, velocity, and acceleration magnitudes in the longitudinal direction. The top panel (Figure 20 (a)) shows the smoothed distance to intersection over time; it ends at zero as the vehicle comes to a stop. The middle panel (Figure 20 (b)) illustrates both raw and smoothed longitudinal velocity over time; the smoothing technique significantly reduces noise while preserving key trends such as deceleration during braking events. The bottom panel (Figure 20 (c)) displays

longitudinal acceleration along with their projections onto the longitudinal direction (negative values indicate deceleration). This projection ensures that acceleration values are consistent with the vehicle's actual motion dynamics.

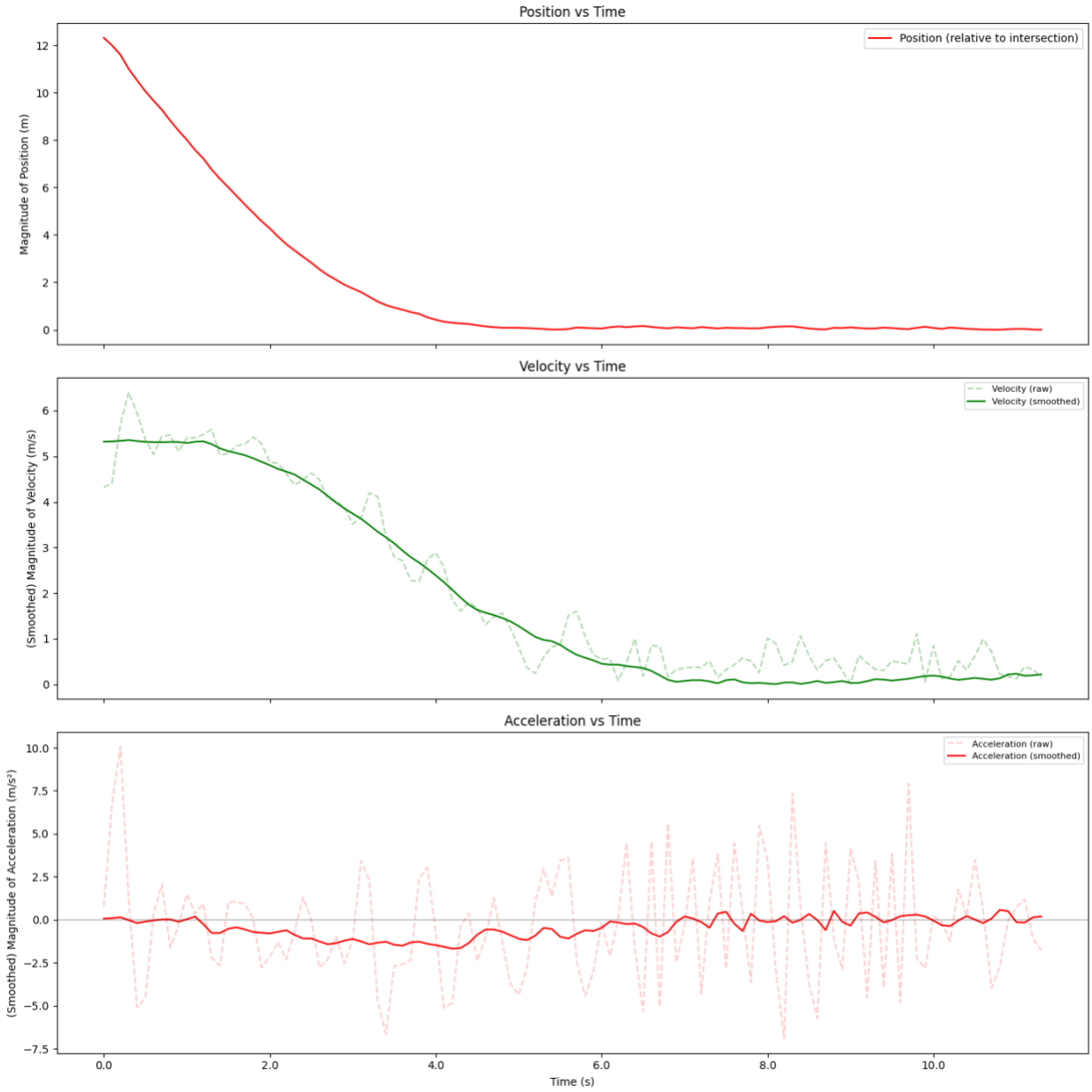

Figure 20. Smoothed trajectory features – (a) XY position magnitude, (b) XY velocity magnitude, and (c) acceleration magnitude with projections onto longitudinal direction.

These results demonstrate how the trajectory refinement process transforms noisy raw detections into accurate representations of vehicle motion dynamics. By providing precise position, velocity, and acceleration information over time, this process enables detailed analyses of braking events and their associated emissions under real-world traffic conditions.

Brake activity detection results

The brake activity detection model was evaluated on two datasets to assess its ability to detect braking events and estimate brake intensity. The first dataset, the probe vehicle dataset, provided detailed time-series measurements, including brake pressure, allowing for a direct comparison between predicted and observed braking intensity. The second dataset, the real-world validation dataset, lacked brake pressure information, requiring the use of alternative metrics such as confusion matrix to evaluate performance. These evaluations demonstrate the model's robustness across diverse conditions and its ability to generalize to a larger size of real-world dataset.

Evaluation on probe vehicle dataset

The probe vehicle dataset captures seven key parameters over a 698-second period, providing high-resolution operational and positional data. Below is a structured list of the recorded variables:

- **Time**: Recorded in Coordinated Universal Time (UTC) for synchronization accuracy.
- **Brake Pressure**: Measured in pounds per square inch (psi) via hydraulic line sensors.
- **Brake Status**: Binary indicator (activated/deactivated) based on pedal position.
- **Latitude/Longitude**: GNSS-derived coordinates using the WGS84 geodetic datum.
- **Speed**: Calculated from wheel sensor data, reported in meters per second (m/s).
- **Altitude**: Barometric elevation measurement in meters (m) above sea level.

This dataset was used to train the hybrid physical-machine learning model and subsequently test it on a separate subset of data to evaluate its predictive accuracy. The results from this evaluation highlight the model's ability to accurately detect braking events and estimate brake intensity. The Mean Squared Error (MSE) for acceleration was 0.247, indicating a strong alignment between predicted and observed deceleration profiles. Similarly, the Root Mean Squared Error (RMSE) for brake pressure was 113.968 PSI, which is acceptable given the typical range of 0–4000 PSI for brake pressure values. These metrics confirm that the model effectively captures braking dynamics under real-world driving conditions.

The evaluation was conducted on an 18-second data segment sampled at 10 Hz, yielding 180 temporal instances demonstrated accurate detection capabilities. The model achieved a precision of 0.9024 and perfect recall (1.000), yielding an F1 score of 0.9487. Quantitative accuracy reached 0.9551, indicating that 95.51% of temporal instances were

correctly classified as braking or non-braking states. This performance profile confirms the system's capacity to identify all true braking events while maintaining a low false positive rate of 4.76% (derived from precision metrics). The 18-second evaluation window contained 42 distinct braking events across varying pressure ranges, providing statistically significant validation of the detection reliability under operational conditions.

Figure 21 provides a detailed visualization of a representative test run from the probe vehicle dataset. Figure 21 (a) shows how distance to stop-bar decreases over time as the vehicle decelerates to a stop, offering an overview of its travel path during braking events. Figure 21 (b) depicts speed fluctuations during these events, illustrating how velocity decreases over time in response to braking activity. Figure 21 (c) overlays total acceleration with both predicted and actual brake pressure on a dual-axis plot. The strong agreement between predicted and actual values validates the model's ability to isolate braking-induced deceleration from other components of total acceleration.

These results affirm that the hybrid physical-machine learning framework is capable of accurately detecting braking events and estimating brake intensity under real-world driving conditions where detailed measurements are available.

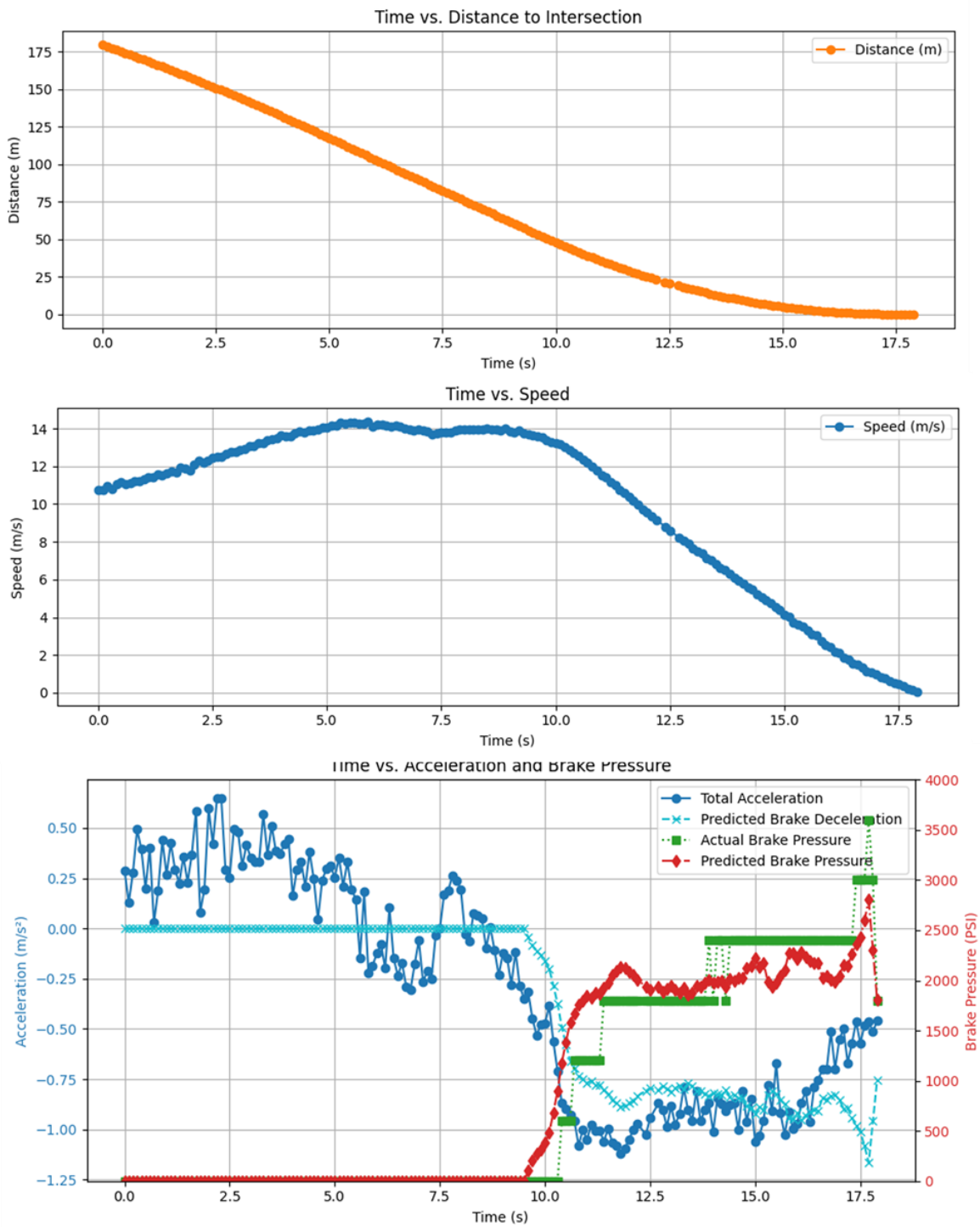

Figure 21. (A) Distance (to the stop-bar), (b) speed, (c) acceleration, and brake pressure over time during a representative probe vehicle test run.

Evaluation on roadside sensor dataset

To assess the model's performance in scenarios where detailed onboard data such as brake pressure is unavailable, the roadside sensor dataset was used. This dataset included trajectory features such as speed and acceleration derived from LiDAR-based trajectories as well as binary brake status obtained from brake light activations.

Unlike the probe vehicle dataset, this roadside sensor dataset lacked direct measurements of brake intensity (pressure or brake-induced deceleration), making it impossible to directly compare predicted brake intensities against ground truth values. Instead, confusion matrix—the proportion of observed braking events captured by the model—was used as an indicator of performance alongside standard event detection metrics such as precision and recall.

The results demonstrate that even without access to direct brake pressure data, the model performs well in detecting braking events based solely on trajectory features. The confusion matrix was high, indicating that most observed braking events (as indicated by brake light activations) were successfully identified by the model. Precision remained at 1.000, meaning all predicted braking events corresponded to actual observations without any false positives. Recall was slightly lower (0.873) due to some missed detections (false negatives), resulting in an overall F1 Score of 0.932.

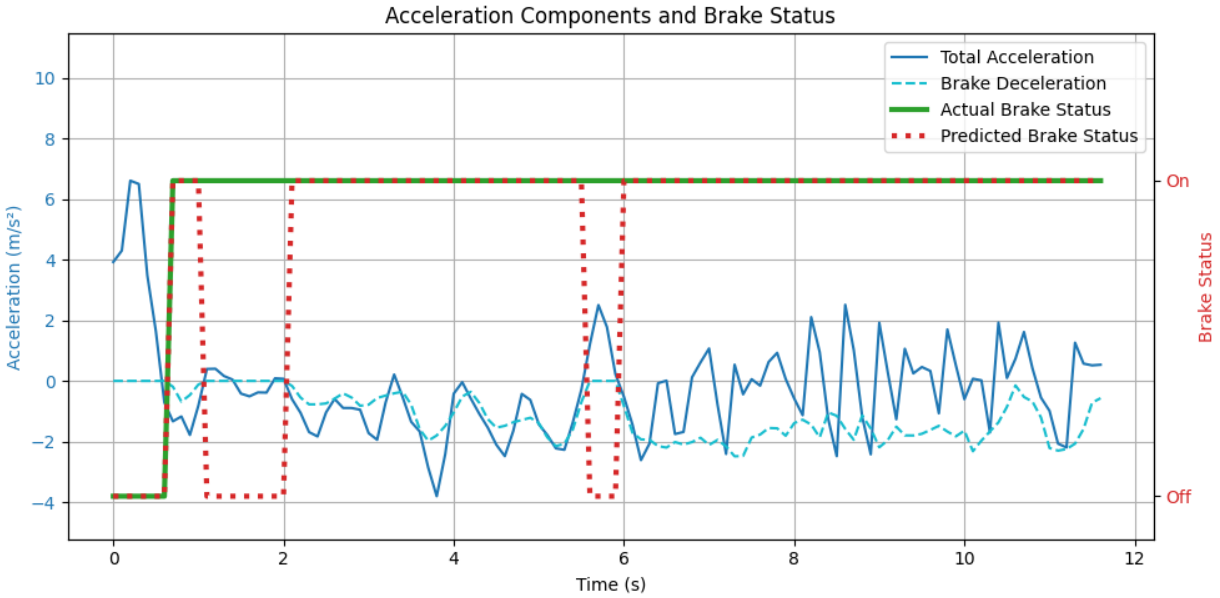

Figure 22. Acceleration and binary brake status on real-world dataset.

Figure 22 illustrates these findings through a detailed visualization of acceleration components and binary brake status during a validation run. The left y-axis shows total acceleration alongside smoothed braking-induced deceleration over time, while the right y-axis compares actual (ground truth) and predicted binary brake statuses (on/off). In the

plot, the predicted brake status (red dotted line) closely follows the actual brake status (green solid line), but slight discrepancies are observed. These discrepancies can be attributed to the limitations of the brake detection model, particularly its inability to classify certain brake events when the total acceleration is greater than 0. The alignment between predicted and actual statuses demonstrates that even without access to direct measurements from OBD-II or brake pressure data, the model effectively identifies braking events based on trajectory features alone.

The findings demonstrate that the brake activity detection model performs robustly across both datasets, showcasing its ability to detect braking events and estimate deceleration under varying conditions. On the probe vehicle dataset, the model accurately captured braking dynamics, achieving high precision and recall while providing reliable estimates of brake intensity. The inclusion of detailed measurements, such as brake pressure, allowed for a direct comparison between predicted and observed braking behavior, validating the model's predictive accuracy. In contrast, the real-world validation dataset, which lacked brake pressure information, relied on alternative metrics like confusion matrix to evaluate performance. Despite these limitations, the model maintained strong precision and reasonable recall, effectively identifying braking events based solely on trajectory features. This adaptability highlights the framework's potential for deployment in real-world traffic monitoring systems where detailed onboard data may not be available. In summary, the results confirm that the hybrid physical-machine learning framework is both accurate and versatile, capable of addressing diverse data scenarios while maintaining reliable performance. These findings underscore the model’s capability for real-world applications such as traffic safety analysis and non-tailpipe emissions estimation.

Brake emission estimation results

The brake emission estimation model quantifies particulate matter (PM10) emissions generated during braking events by leveraging vehicle trajectory data and a calibrated empirical emission factor k. The results will demonstrate the model's ability to estimate emissions under real-world conditions and highlight material-specific variations in brake wear emissions.

Calibration of the Empirical Emission Factor

The empirical emission factor k, which relates kinetic energy dissipation during braking to PM10 emissions, was calibrated using dynamometer test data [26] for different brake pad materials. Figure 23 illustrates the calibration results, showing the relationship between predicted brake emissions PM10 and measured PM10 emission factors for materials such as ECE, NAO, semi-metallic, and others.

The linear regression analysis yielded the following k values:

- ECE: $3.57 * 10^{-5} mg \cdot s^2/kg \cdot m^2$
- NAO: $1.03 * 10^{-5} mg \cdot s^2/kg \cdot m^2$
- Semi-metallic: $1.45 * 10^{-5} mg \cdot s^2/kg \cdot m^2$
- Other: $1.88 * 10^{-5} mg \cdot s^2/kg \cdot m^2$

These results highlight significant material-specific variations in PM10 emissions. ECE materials exhibit the highest k, indicating greater particulate generation per unit of energy dissipated, while NAO materials have the lowest k, reflecting reduced PM10 emissions. Semi-metallic and "Other" materials fall between these extremes. The calibration process confirms that material composition plays a critical role in determining brake wear particulate emissions. The calibrated k values were subsequently used to estimate brake emissions in real-world scenarios.

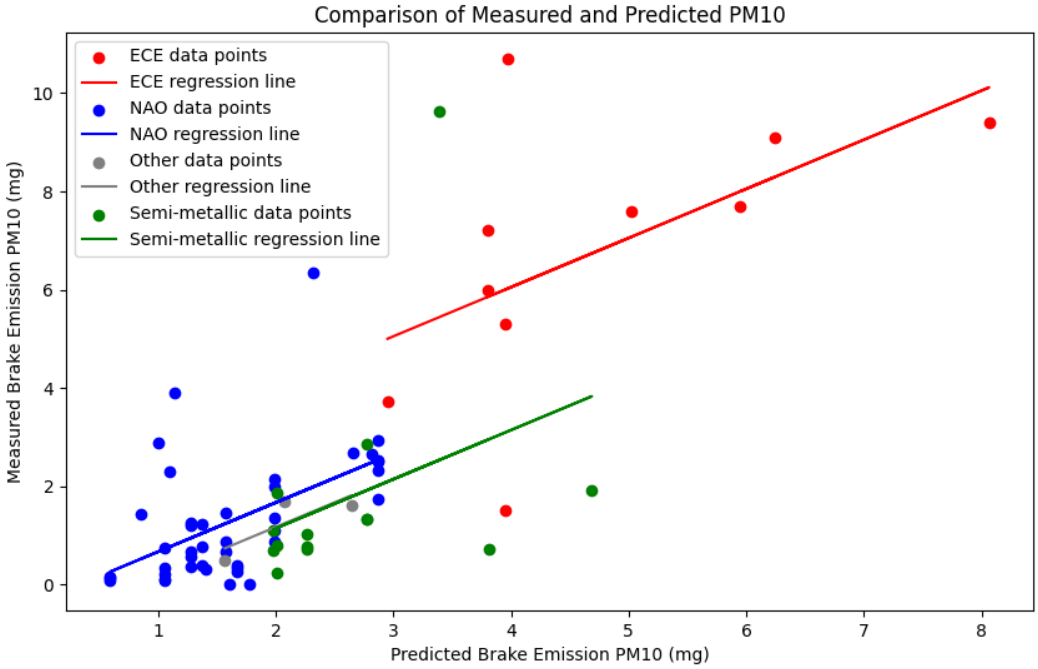

Figure 23. Empirical emission factor calibration.

Real-world estimation of brake emissions

Using the calibrated k value for NAO brake pads, the model was applied to LiDAR-detected vehicle trajectories to estimate PM10 emissions during braking events. Figure 24 shows cumulative PM10 emissions over time for a representative braking event of the trip shown in Figure 22. The cumulative emissions increase steadily as braking progresses, with a total of approximately 0.2 micrograms of PM10 emitted over a 12-second period. This result demonstrates the model's ability to capture transient emission patterns with high temporal resolution. By integrating LiDAR-based trajectory data with calibrated k values,

the framework provides detailed insights into non-tailpipe emissions under diverse traffic conditions.

In summary, the brake emission estimation results validate the proposed framework's effectiveness in quantifying non-tailpipe emissions:

- The calibration process established material-specific k values, enabling accurate estimation of PM10 emissions across different brake pad types.
- Real-world application using LiDAR-detected trajectories demonstrated the model's ability to estimate cumulative emissions with high temporal granularity.

These findings underscore the importance of considering material-specific variations when estimating non-tailpipe emissions and highlight the potential of this approach for improving emission inventories and informing regulatory policies aimed at mitigating particulate matter pollution from braking systems.

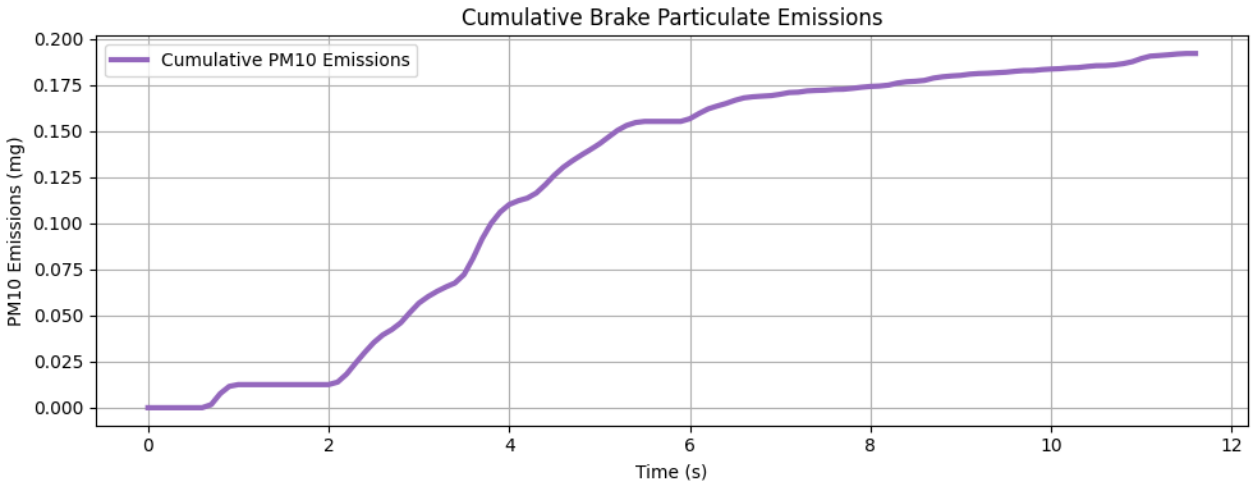

Figure 24. Cumulative brake emission on real world dataset.

Discussion

To conclude this report, a few pertinent aspects are further discussed below.

Limited detection range of LiDAR

The LiDAR sensor installed at the intersection provided reliable detection results for vehicles only within approximately 40 meters of the intersection. This limited range meant that some vehicles may have already initiated braking before entering the detection zone, resulting in incomplete data on the full braking event. Consequently, the system was unable to capture the initiation and progression of braking, which needs careful interpretation of vehicle brake activity and associated emissions.

Material-specific emission variations

Brake emissions vary significantly based on the material composition of brake pads. For example, ECE brake pads tend to produce higher particulate matter emissions compared to NAO and semi-metallic pads. These material-specific differences are critical for accurately modeling non-tailpipe emissions. However, LiDAR-based systems are unable to detect or differentiate emissions based on brake pad materials, as they rely solely on trajectory data and cannot capture chemical or physical properties of emitted particles. This limitation highlights the need for complementary methods, such as laboratory testing or onboard sensors, to integrate material-specific emission factors into real-world applications and analyses.

Regenerative braking and powertrain differentiation Challenges

The data collected in this study was sourced from an internal combustion engine (ICE) vehicle, which relies exclusively on friction brakes. While electric vehicles (EVs) equipped with regenerative braking systems may significantly reduce reliance on friction brakes, this study's LiDAR-based detection system cannot differentiate between ICEVs and EVs. As a result, regenerative braking effects—such as reduced brake emissions—are not accounted for in the analysis. This limitation restricts the applicability of findings to mixed traffic scenarios where EV adoption is increasing and underscores the need for future studies to incorporate methods capable of distinguishing vehicle types and braking technologies, such as automated license plate recognition.

References

[1] C. Lin, G. Sun, D. Wu, and C. Xie, "Vehicle detection and tracking with roadside LiDAR using improved ResNet18 and the Hungarian algorithm," Sensors, vol. 23, no. 19, p. 8143, 2023.

[2] Z. Bai, G. Wu, M. J. Barth, Y. Liu, E. A. Sisbot, and K. Oguchi, "Pillargrid: Deep learning-based cooperative perception for 3d object detection from onboard-roadside lidar," in 2022 IEEE 25th International Conference on Intelligent Transportation Systems (ITSC), 2022, pp. 1743–1749, IEEE.

[3] F. Guan, H. Xu, and Y. Tian, "Evaluation of roadside LiDAR-based and vision-based multi-model all-traffic trajectory data," Sensors, vol. 23, no. 12, Art. no. 5377, 2023.

[4] Z. Bai, S. P. Nayak, X. Zhao, G. Wu, M. J. Barth, X. Qi, et al., "Cyber mobility mirror: A deep learning-based real-world object perception platform using roadside LiDAR," IEEE Transactions on Intelligent Transportation Systems, vol. 24, no. 9, pp. 9476-9489, 2023.

[5] P. Mohan, V. N. Padmanabhan, and R. Ramjee, "Nericell: rich monitoring of road and traffic conditions using mobile smartphones," in Proceedings of the 6th ACM Conference on Embedded Network Sensor Systems, 2008, pp. 323–336.

[6] A. Kazemeini, I. Taheri, and A. Samimi, "A GPS-based algorithm for brake and turn detection," International Journal of Intelligent Transportation Systems Research, vol. 20, no. 2, pp. 433–445, 2022.

[7] J. R. Palit and O. A. Osman, "Application of LiDAR data for deep learning based near crash prediction at signalized intersection," Journal of Transportation Technologies, vol. 13, no. 2, pp. 158-172, 2023.

[8] E. Jiang and X. Wang, "Analysis of abnormal vehicle behavior based on trajectory fitting," Journal of Computer and Communications, vol. 3, no. 11, pp. 13–18, 2015.

[9] W. Sawczuk, A. Merkisz-Guranowska, A.-M. Rilo Cañás, and S. Kołodziejski, "New approach to brake pad wear modelling based on test stand friction-mechanical investigations," Eksploatacja i Niezawodność, vol. 24, no. 3, 2022.

[10] T. Grigoratos and G. Martini, "Non-exhaust traffic related emissions. Brake and tyre wear PM," Eur. Commission, JRC Sci. Policy Rep., Luxembourg, Rep. EUR 26648, 2014.

[11] H. Hagino, "Brake wear and airborne particle mass emissions from passenger car brakes in dynamometer experiments based on the worldwide harmonized light-duty vehicle test procedure brake cycle," Lubricants, vol. 12, no. 6, p. 206, 2024.

[12] T. Grigoratos and G. Martini, "Brake wear particle emissions: a review," Environmental Science and Pollution Research, vol. 22, pp. 2491–2504, 2015.

[13] B. Lopez, K. Johnson, and H. Jung, "Development of brake activity measurement method for heavy-duty vehicles," J. Air Waste Manage. Assoc., vol. 73, no. 7, pp. 568-577, 2023.

[14] California Air Resources Board, "Brake and Tire Wear Emissions: Final Report, Revision 2," prepared by Eastern Research Group in cooperation with LINK Testing Laboratories, Inc., Feb. 11, 2021. [Online]. Available: https://ww2.arb.ca.gov/sites/default/files/2021-04/17RD016.pdf

[15] M. Tutuianu et al., "Development of the World-wide harmonized Light duty Test Cycle (WLTC) and a possible pathway for its introduction in the European legislation," Transp. Res. D Transp. Environ., vol. 40, pp. 61-75, 2015.

[16] M. Mathissen, J. Grochowicz, C. Schmidt, R. Vogt, F. H. F. zum Hagen, T. Grabiec, H. Steven, and T. Grigoratos, "A novel real-world braking cycle for studying brake wear particle emissions," Wear, vol. 414, pp. 219–226, 2018.

[17] P. G. Sanders, N. Xu, T. M. Dalka, and M. M. Maricq, "Airborne brake wear debris: size distributions, composition, and a comparison of dynamometer and vehicle tests," Environmental Science & Technology, vol. 37, no. 18, pp. 4060–4069, 2003.

[18] R. M. Harrison, A. M. Jones, J. Gietl, J. Yin, and D. C. Green, "Estimation of the contributions of brake dust, tire wear, and resuspension to nonexhaust traffic particles derived from atmospheric measurements," Environ. Sci. Technol., vol. 46, no. 12, pp. 6523-6529, 2012.

[19] J. Chen et al., "Mining urban sustainable performance: GPS data-based spatio-temporal analysis on on-road braking emission," J. Clean. Prod., vol. 270, p. 122489, 2020.

[20] B. Giechaskiel, T. Grigoratos, P. Dilara, T. Karageorgiou, L. Ntziachristos, and Z. Samaras, "Light-duty vehicle brake emission factors," Atmosphere, vol. 15, no. 1, Art. no. 97, 2024.

[21] B. D. Garg, S. H. Cadle, P. A. Mulawa, P. J. Groblicki, C. Laroo, and G. A. Parr, "Brake wear particulate matter emissions," Environ. Sci. Technol., vol. 34, no. 21, pp. 4463-4469, 2000.

[22] H. Hagino, M. Oyama, and S. Sasaki, "Laboratory testing of airborne brake wear particle emissions using a dynamometer system under urban city driving cycles," Atmospheric Environment, vol. 131, pp. 269–278, 2016.

[23] C. Agudelo, R. T. Vedula, S. Collier, and A. Stanard, "Brake particulate matter emissions measurements for six light-duty vehicles using inertia dynamometer testing," SAE International Journal of Advances and Current Practices in Mobility, vol. 3, no. 2020-01-1637, pp. 994–1019, 2020.

[24] D. P. Kingma and J. Ba, "Adam: A method for stochastic optimization," arXiv preprint arXiv:1412.6980, 2014.

[25] U.S. Environmental Protection Agency, "Motor Vehicle Emission Simulator: MOVES5," Office of Transportation and Air Quality, Ann Arbor, MI, Nov. 2024.

[26] Q. Chen and R. Tu, “Brake Wear Particle Emission Factors from Dynamometer Tests,” Mendeley Data, V1, 2024. doi: 10.17632/crxjtgk5bg.1.

Data Summary

Products of Research

The dataset compiles multi-sensor data collected to analyze vehicle braking events and associated non-tailpipe particulate matter emissions at urban intersections. The data sources include GPS logs, LiDAR point clouds, video recordings, and onboard vehicle sensors. These data support research on vehicle dynamics, braking behavior analysis, trajectory refinement, and emission estimation.

Data Format and Content

The dataset consists of various file formats and contents:

- CSV Files: Processed probe vehicle data with variables such as time, acceleration, speed, distance traveled, brake pressure, and brake status.
- UBX Files: Raw GPS data collected by a u-blox GPS receiver.
- Compressed Archives (7z): Contains raw LiDAR point cloud data (DB3 format) and detection bounding box results.
- MOV and MP4 Video Files: Video recordings captured by roadside cameras and drones.
- TXT Files: Brake status and pressure data.
- Refined Trajectory Files (CSV): Labeled brake status data derived from LiDAR detections.

Each file includes metadata such as timestamps, location coordinates (latitude/longitude), speed, altitude, and braking details.

Data Access and Sharing

The dataset is publicly accessible through Dryad at the following DOI: https://doi.org/10.5061/dryad.41ns1rnrp. Users can download the data directly from this repository without restrictions.

Reuse and Redistribution

The dataset is currently private and will remain so during the peer review process of the related article. During this period, access to the dataset is restricted, but it can be shared with collaborators or other authorized individuals using a private URL provided by Dryad. The dataset will not be publicly available or evaluated by curators until the authors choose to release it from this status.

Once the dataset is made public, users will be required to:

- Cite the dataset's DOI in any publications or presentations derived from its use.
- Follow any additional terms of use specified at the time of public release.

For further inquiries or to request access during the private phase, please contact the dataset's authors directly.

Citation for the Dataset

Zhao, Xuanpeng; Wu, Guoyuan; Jung, Heejung; Anubolu, Ajay. Data for Understanding Real-World Brake Activity: A Key to Assessing Non-Tailpipe Emission Sources. Dryad Digital Repository. DOI: https://doi.org/10.5061/dryad.41ns1rnrp.